

Check for updates

An Overview of Flame-Retardant Materials for Triboelectric **Nanogenerators and Future Applications**

Swati Panda, Sugato Hajra, Hyeonggeun Kim, Jeonggyu Seo, ByeongJun Jeong, Ingyu Lee, Kushal Ruthvik Kaja, Mohamed Ahmed Belal, Venkateswaran Vivekananthan, Hamideh Khanbareh, Chris Bowen, Krystian Mistewicz, and Hoe Joon Kim*

Triboelectric nanogenerators (TENGs) have gained significant attention for ability to convert mechanical energy into electrical energy. As the applications of TENG devices expand, their safety and reliability becomes priority, particularly where there is risk of fire or spontaneous combustion. Flame-retardant materials can be employed to address these safety concerns without compromising the performance and efficiency of TENGs. The primary focus of this review is on flame-retardant materials, including polymers, biomaterials, liquid polymers, aerogels, and carbon-based materials. The fundamental properties of these materials for TENG applications are elucidated. The characteristics of each material type are described, along with their potential to boost the safety and performance of TENGs. The importance of flame retardancy in advancing TENG technology can be projected from its usage in wearable electronics, self-powered sensors, and smart textiles. Current challenges such as material compatibility, fabrication complexity, and environmental concerns are addressed, along with proposed strategies for overcoming them. This review underscores the significance of flame-retardant materials in strengthening the functionality and safety of TENG devices, paving the way for their widespread adoption across various industries.

S. Panda, S. Hajra, H. Kim, J. Seo, B. Jeong, I. Lee, K. R. Kaja, M. A. Belal, H. J. Kim

Department of Robotics and Mechatronics

Daegu Gyeongbuk Institute of Science and Technology (DGIST)

Daegu 42988, South Korea E-mail: joonkim@dgist.ac.kr

V. Vivekananthan

Center for Flexible Electronics

Department of Electronics and Communication Engineering

Konery Lakshmaiah Education Foundation

Guntur, Andhra Pradesh 522302, India

H. Khanbareh, C. Bowen

Department of Mechanical Engineering

University of Bath

Bath BA2 7AY, UK

K. Mistewicz

Institute of Physics - Centre for Science and Education Silesian University of Technology

Krasińskiego 8, Katowice 40-019, Poland





© 2025 The Author(s). Advanced Materials published by Wiley-VCH GmbH. This is an open access article under the terms of the Creative Commons Attribution License, which permits use, distribution and reproduction in any medium, provided the original work is properly cited.

DOI: 10.1002/adma.202415099

1. Introduction

TENGs are energy harvesting devices that generate electrical energy without the need for an external power source by converting various mechanical vibrations into electrical energy.[1-4] The fundamental principle of TENG operation involves a combination of contact electrification and electrostatic induction. Contact electrification generates static polarized charges, while electrostatic induction is the primary process that converts mechanical energy into electricity. Their versatility, scalability, and potential for creating self-powered systems have sparked considerable interest across diverse fields ranging from wearable electronics to environmental sensing.[5-10] However, as TENG applications expand, ensuring the safety and reliability of these devices becomes increasingly critical, particularly in environments where there is a risk of fire or ignition.[11-13] Flame-retardant materials present a compelling solution to address

these safety challenges, while maintaining the high performance and efficiency of TENGs. [14,15] These materials possess intrinsic properties or additives that inhibit or delay the spread of flames, thereby reducing the risk of fire-related hazards.[16-18] By integrating flame-retardant materials into TENG design and fabrication, researchers aim to enhance the safety and reliability of these devices, enabling their deployment in a broader range of applications.[12,19-23]

Polymers constitute the backbone of the majority of TENG devices due to their mechanical flexibility, durability, and ease of processing.[24-26] Various flame-retardant additives, such as phosphorus-based compounds, halogen-containing compounds, and intumescent agents, have been explored for their efficacy in enhancing the flame retardancy of polymer-based TENGs.^[27–30] Additionally, biomaterials derived from natural sources, such as cellulose and chitosan, offer sustainable alternatives with inherent flame-retardant properties, thereby opening new avenues for eco-friendly TENG applications.[31-34] Liquid polymers, including silicone-based materials and hydrogels, also present intriguing opportunities for improving TENG flexibility and conformability while imparting flame retardancy.[35,36] Moreover, aerogels demonstrate exceptional thermal insulation properties and high surface area, making them attractive candidates for

www.advmat.de

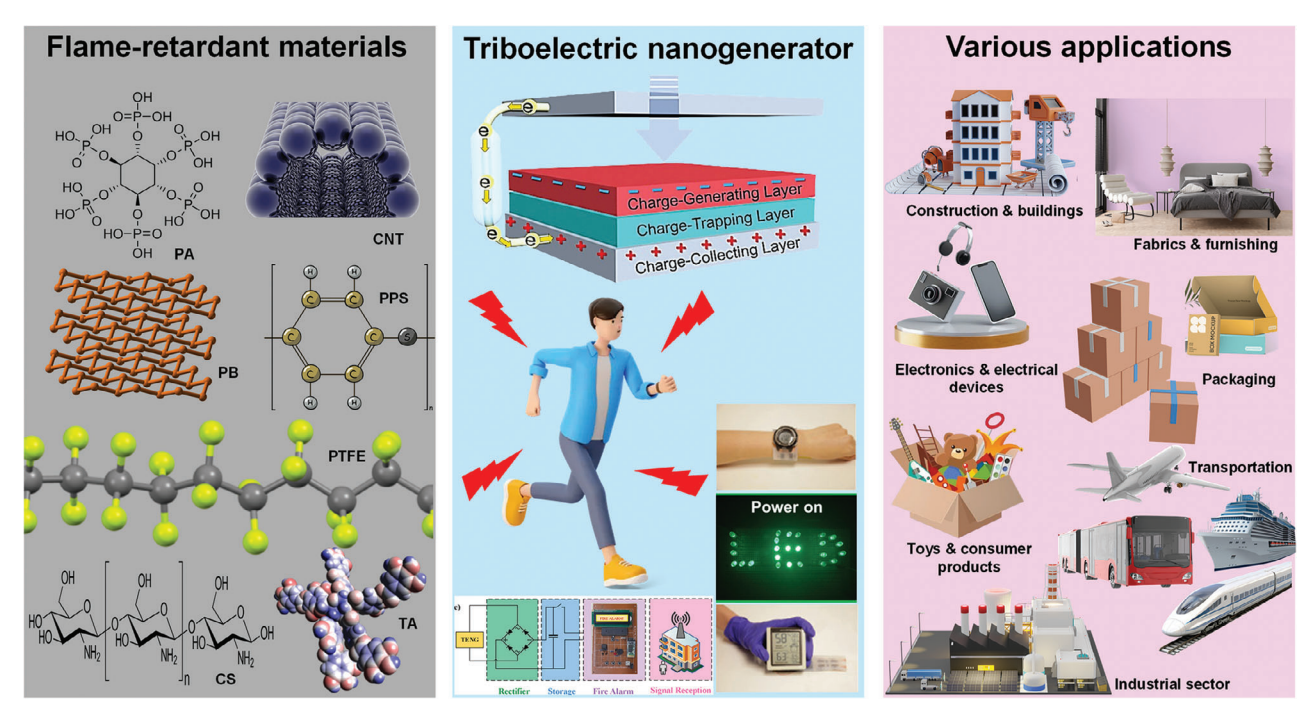


Figure 1. Overview of flame-retardant materials, the triboelectric nanogenerator, and their applications.

flame-retardant TENG encapsulation and insulation.^[37–40] Furthermore, carbon-based materials, such as graphene and carbon nanotubes, have high conductivity and mechanical strength, thereby enhancing TENG performance.^[41–44]

This review highlights recent progress in the area of flameretardant materials employed in TENGs and their applications. The discussion encompasses a broad spectrum of flameretardant materials, highlighting their unique properties and suitability for TENG integration. Each material type is analyzed in detail to elucidate its flame-retardant mechanism, compatibility with TENG fabrication processes, and potential impact on device performance. In addition to overviewing the fundamental properties of flame-retardant materials, this review explores their potential applications in TENG-based technologies. Wearable electronics, self-powered sensors, and structural health monitoring systems are identified as key areas where flame-retardant TENGs could offer significant advantages in terms of safety, reliability, and energy autonomy. However, despite the promising advancements, several challenges remain that must be addressed to fully realize the potential of flame-retardant TENGs; these include material compatibility, fabrication complexity, and environmental

In summary, this review aims to provide insights into the recent progress, challenges, and future directions in flame-retardant materials for TENG applications. By elucidating the diverse range of materials and their potential impact on TENG performance and safety, this review seek to inspire further research and innovation in this rapidly evolving field. Ultimately, the integration of flame-retardant materials holds the key to unlocking the full potential of TENG technology and enabling its widespread adoption in various industrial and consumer applications. Figure 1 presents a schematic overview of the range

of flame-retardant materials, the TENG, and their potential applications.

2. Working Mechanism of the Triboelectric Nanogenerator (TENG)

The working mechanism of a TENG involves several key steps. First, when two materials come into touch, contact electrification takes place, producing both positive and negative charges as per the polarity of each material.[45,46] Upon separation of the two materials, these charges become spatially distributed on their surfaces, creating an electric field between them.^[47,48] The potential difference induces charge transfer to nearby conductive electrodes, thereby generating an electric current that can flow through an external circuit.[49,50] When the materials are brought back into contact, the cycle repeats, allowing for continuous energy generation.^[51,52] The key components of a TENG include the triboelectric layer, responsible for contact electrification and charge transfer, and conductive electrodes placed near the triboelectric layer to collect and transfer the generated charges.^[53–55] The external *electrical load*, such as a resistor or electronic device, utilizes the electrical energy produced by the TENG. The contact separation mode is the most basic and primary type of TENG, as illustrated in Figure 2a.[56]

The surfaces of two dielectrics become charged when they come into contact. The two surfaces of dielectrics retain charge after separation, creating a potential difference between the materials.^[57,58] An electrostatic field transfers electric charge from one electrode to another. The electrostatic field dissipates when the materials come into contact again, allowing the electrons to return. ^[59,60] This repetitive process produces an alternating current (AC). ^[61,62] Figure 2b shows an output node related

15214095, 2025, 9, Downloaded from https://adv.

onlinelibrary.wiley.com/doi/10.1002/adma.202415099 by Dægu Gyeongbuk Institute Of, Wiley Online Library on [20/03/2025]. See the Terms and Conditions (https://onlinelibrary.wiley.com/terms

and-conditions) on Wiley Online Library for rules of use; OA articles are governed by the applicable Creative Commons

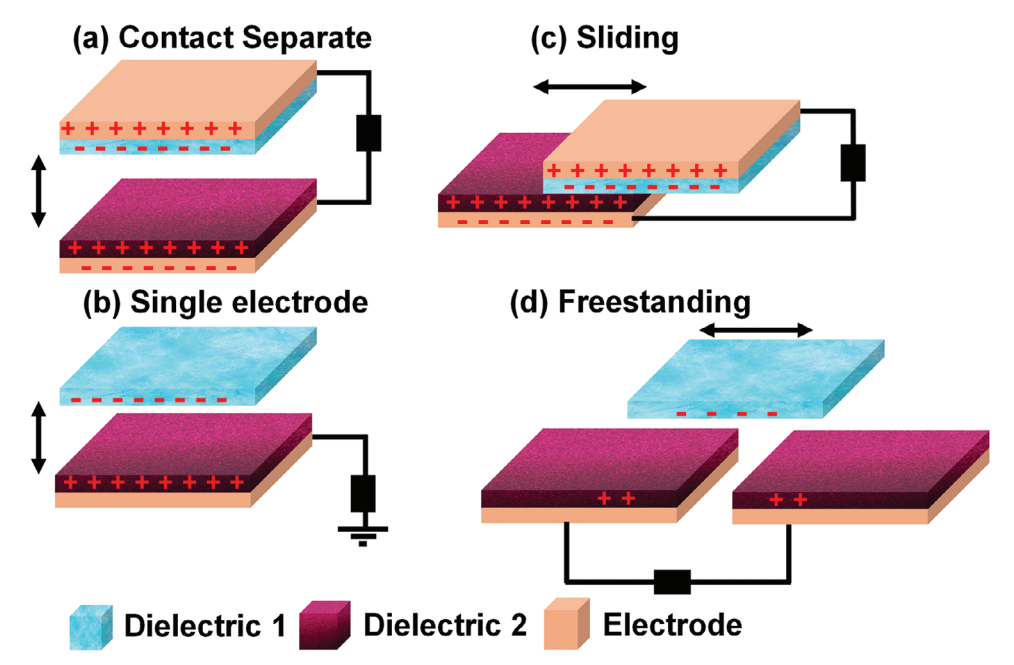


Figure 2. Four classical working modes of TENGs a) Contact separation mode. b) Single electrode mode. C) Sliding mode. d) Freestanding mode.

to a single electrode, while the other node remains grounded, allowing for simple operation. In contrast, the two-electrode arrangement, which connects two output nodes to each electrode, allows for greater motion.^[63,64]

The sliding mode primarily deals with rotating or translating motion via friction. The two objects in contact do not separate but instead move with a differing contact area, as illustrated in Figure 2c. [65,66] During frictional sliding, triboelectric charges are formed on the surfaces of the two dielectrics, resulting in a potential difference between the electrodes. [67-69] At this point, the potential difference fluctuates based on the effective contact area, and this cycle also generates an alternating current.[70,71] The freestanding mode relies on a natural interaction between a moving triboelectric layer (TL) and the surrounding matter (Figure 2d), such as air.^[72] In previous modes, the triboelectric layer was artificially charged through purposeful friction between two dielectrics; in this mode, it self-charges as a result of natural friction. Furthermore, it does not require periodic electrification through external mechanical control since charges on the triboelectric layer can be maintained for extended periods. [73,74] Due to the uneven movement of the moving triboelectric layer, an asymmetric electric field is created between the two materials that varies with the distance between the electrode and the charged material. This asymmetrical electric field leads to the flow of electrical charges and causes triboelectricity. Unlike the prior modes, this mode eliminates direct material contact, resulting in fewer areas of wear.^[74,75] Although there is minimal voltage generation, this mode of operation can enhance the longevity of the triboelectric layer.[76,77]

3. Mechanism of Flame-Retardant

Flame-retardant materials function by disrupting the combustion process through physical and chemical mechanisms. These

mechanisms can act in one or more stages of combustion: heating, ignition, flame propagation, and decomposition.^[78,79] The primary flame-retardant mechanisms are discussed below:

3.1. Endothermic Decomposition

Some flame-retardant materials decompose endothermically (absorbing heat) when exposed to high temperatures. [80,81] This process reduces the heat available to sustain the combustion reaction, lowering the temperature of the material and slowing or stopping the fire. For example, aluminum hydroxide (Al(OH) $_3$) and magnesium hydroxide (Mg(OH) $_2$) decompose endothermically, releasing water vapor, which cools the material and dilutes combustible gases.

3.2. Formation of a Protective Char Layer

On the surface of some flame-retardant materials, a layer of carbonaceous char is encouraged to form. This char slows down gas release and thermal degradation by protecting the underlying material from heat and oxygen. [82,83] Phosphorus-based flame retardants, which form phosphoric acid, are the primary examples that promote char formation by dehydrating the material.

3.3. Dilution of Combustible Gases

Some flame-retardant materials release inert gases (such as nitrogen, water vapor, or carbon dioxide) when heated. [84] These gases dilute the concentration of flammable gases (such as volatile organic compounds) around the material, making it harder for the fire to sustain itself. [85] For example, ammonium polyphosphate (APP) releases water vapor and nitrogen, which dilute the oxygen around the flame.





3.4. Gas Phase Inhibition (Free Radical Scavenging)

In the gas phase, flame-retardant materials can interfere with the flame propagation chemistry by capturing and neutralizing highly reactive radicals (such as H and —OH) that are critical to sustaining combustion. [86,87] Halogenated flame retardants, such as brominated or chlorinated compounds, release halogen radicals that scavenge the reactive radicals in the flame, thereby slowing down or stopping the combustion reaction. [88]

3.5. Formation of a Ceramic Barrier

Certain flame-retardant materials can form a non-combustible, glass-like ceramic barrier when exposed to high temperatures. This layer shields the material from heat and oxygen, helping to suppress further combustion. [89,90] For example, intumescent flame retardants expand to form a foamy, insulating layer when heated, creating a protective barrier.

4. Material Properties and Characterization Techniques

Flame-retardant materials play a critical role in enhancing fire safety across numerous industries, including construction, transportation, and electronics.[91] These materials are designed to inhibit or delay the spread of flames, thereby reducing the risk of fire-related accidents and minimizing property damage. Several important properties characterize flame-retardant materials, and their characterization is essential for evaluating their effectiveness and suitability for specific applications. The primary property of flame-retardant materials is their ability to suppress or slow down the combustion process when exposed to heat or flames.^[92] This is typically assessed through standardized tests such as the UL 94 (Underwriters Laboratories Standard for Safety of Flammability of Plastic Materials) or ASTM E84 (Standard Test Method for Surface Burning Characteristics of Building Materials). Flame-retardant materials must possess high thermal stability, enabling them to withstand elevated temperatures without undergoing significant degradation. Thermogravimetric analysis (TGA) and differential scanning calorimetry (DSC) provide insights into the endurance of materials under various thermal conditions by measuring their weight loss and heat flow as a function of temperature, respectively.[93] In addition to inhibiting the spread of flames, flame-retardant materials should minimize the generation of smoke and toxic gases during combustion. Smoke density and toxicity can be evaluated using methods such as the smoke density rating test (ASTM E662) and toxicity screening tests. Flame-retardant materials often form a protective char layer upon exposure to fire, ultimately limiting the combustion process.[94] The cone calorimeter test measures heat release rates (HRR), peak heat release rates (PHRR), and total heat release (THR), providing insights into combustion intensity and material flammability. Oxygen consumption calorimetry also quantifies HRR and THR by tracking oxygen depletion during combustion. The range of properties of flame-retardant materials is overviewed in the schematic presented in **Figure 3**.

X-ray diffraction (XRD) and FTIR examine structural and chemical modifications, while atomic force microscopy (AFM)

and dynamic mechanical analysis (DMA) assess nanoscale surface roughness and viscoelastic properties, respectively. These methods collectively provide a comprehensive understanding of how flame-retardant materials behave under heat, influencing their suitability for triboelectric applications. [95-97] Impedance spectroscopy and LCR meter measure the dielectric constant (permittivity), dielectric loss, and loss tangent over a range of frequencies. This provides insights into how the material stores and dissipates electrical energy, which can be affected by the addition of flame-retardant components, thereby influencing their overall triboelectric performance and suitability for energy harvesting applications. Tensile testing such as stress-strain curves, flexural testing, and impact testing are standard techniques for evaluating mechanical properties. X-ray photoelectron spectroscopy (XPS) and nuclear magnetic resonance (NMR) spectroscopy provide valuable insights into the elemental composition and molecular structure of flame retardants. Flame-retardant materials should be compatible with other components within the system, such as polymers, additives, and processing aids. Compatibility testing involves evaluating factors such as solubility, dispersion, and phase separation using techniques such as microscopy and spectroscopy. [98] By understanding and optimizing these properties, researchers and industry professionals can develop effective flame-retardant materials to mitigate fire hazards in diverse applications.

5. Flame-Retardant Material-Based TENGs

5.1. Conventional Fire-Retardant Polymers

Polymers are preferred for use in various TENGs due to their advantages, such as mechanical flexibility, lightweight nature, ease of manufacturing, and scalability. However, aside from fluorinecontaining polymers such as polyvinylidene fluoride (PVDF), polytetrafluoroethylene (PTFE), and Kapton (polyimide (PI)), many polymeric materials encounter significant issues related to flammability and melt-dripping in response to heat. These challenges have the potential to disrupt electronic devices and pose serious fire hazards.[85,91,99] Therefore, the development of flameretardant triboelectric materials for use in harsh or extreme conditions can be beneficial.[100,101] To enhance the flame resistance of polymers, two primary strategies are employed: reactive-type flame retardants and additive-type flame retardants. The reactive approach involves chemically integrating flame-retardant agents or highly thermally stable structures into the polymer backbone, side chains, or crosslinked networks. This method results in superior flame-retardant effectiveness and extremely high thermal stability.

Chen et al. proposed a facile, robust, and low-cost solution-casting method to prepare a flame-resistant triboelectric polymer of polyvinyl alcohol (PVA) by doping phenyl phosphonic acid (PPA)-polyethyleneimine (PEI) polyelectrolyte synthesized from phenyl phosphonic acid and branched PEI. The PVA/PPA-PEI film containing 10 wt.% PPA-PEI self-extinguished immediately after the flame burner was moved away from the sample, while the neat PVA film burned thoroughly. The PVA/PPA-PEI: PVDF TENG exhibits a higher charge density than the original PVA: PVDF TENG due to the hybrid electron-ion transport ability of the PVA/PPA-PEI film. Moreover, as PPA-PEI

15214095, 2025, 9, Downloaded from https://advanced

onlinelibrary.wiley.com/doi/10.1002/adma.202415099 by Dægu Gyeongbuk Institute Of, Wiley Online Library on [20.03/2025]. See the Terms

and Conditions (https://onlinelibrary.wiley.com/terms-

and-conditions) on Wiley Online Library for rules of use; OA articles are governed by the applicable Creative Commons License

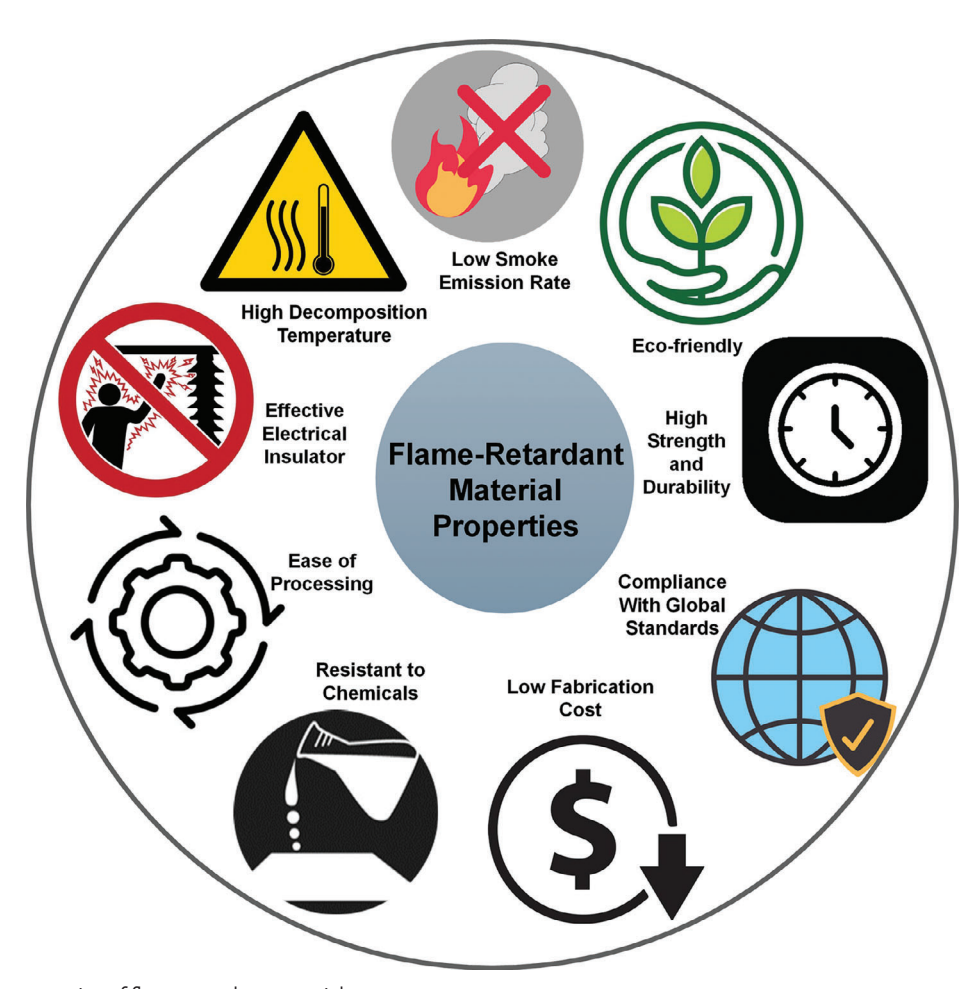


Figure 3. Important properties of flame-retardant materials.

concentrations increase, larger electrical outputs are observed. Two primary factors are related. One is that the amino groups of PPA-PEI can increase the number of electrons supplied during contact electrification, as they are efficient electron donors. The second is that more water is absorbed by the PVA/PPA-PEI surface when the PPA-PEI electrolyte is present. Consequently, a higher concentration of PPA-PEI tends to produce more mobile ions and donate more electrons, resulting in greater surface charge density and increased V_{OC} , I_{SC} , and power or power density. The charge transfer phenomenon is illustrated in **Figure 4a**,b. In addition, the material exhibited a low PHRR of 148.7 \pm 4.2 W g⁻¹, representing a reduction of \approx 47.8%. The effect of temperature on output voltage is shown in Figure 4c,d.

Ma et al. suggested using a new conjugated benzene ring blended with polydimethylsiloxane (PDMS) called PPMS to showcase a fire-resistant TENG. [103] The benzene ring allows the PDMS to achieve superior mechanical properties, high dielectric constant (3.9), anti-dripping functionality, endurance, and fire-retardant behavior. When the TENG was fabricated with PPMS, the mechanism of enhanced electrical performance was revealed through density functional theory simulation methods (Figure 4e). From a molecular perspective, the volume of the Sibenzene group could reach $\approx 29.08 \text{ Å}^3$ that was twice that of Si-

CH₂ (13.86 Å³). Similarly, the energy of Si-benzene (190.6 eV) is significantly higher than that of Si-CH₃ (86.5 eV). When the friction layer comes into contact with PPMS, the collision probability and volume of Si-benzene are higher than the Si-CH₃, improving electrical output performance. Furthermore, when the benzene group approached each other, greater energy was generated compared to the methyl group (Figure 4f). All simulation results demonstrate that the introduction of benzene was beneficial for enhancing the TENG output and performance. As shown in Figure 4g, no melt casting was observed during the burning process, and the PPMS morphology almost maintained its original form within 15 s of burning. However, other polymer materials experienced significant deformation. The blue arrow LED symbol, as seen in Figure 4h, can be illuminated even after 60 seconds of burning, indicating that the safety channel indicator will always beilluminated and will not be affected by the fire. Additionally, the output voltage dropped somewhat from 104 to 98 V. sustaining output voltages of 100% and 80% at high temperatures (300 °C).

Cheng et al. developed a flame-retardant textile-based TENG (FT-TENG) using two flame-retardant cotton fabrics (FC), a PTFE-coated cotton fabric (PC), and a divider, as illustrated in **Figure 5a**,b. $^{[104]}$ The flame -retardant cotton fabric was made by immersing a cotton fabric in a PEI and melamine solution and

15214095, 2025, 9, Downloaded from https://advanced.onlinelibrary.wiley.com/doi/10.1002/adma.202415099 by Dægu Gyeongbuk Institute Of, Wiley Online Library on [20.03/2025]. See the Terms

and-conditions) on Wiley Online Library for rules of use; OA articles are governed by the applicable Creative Commons License

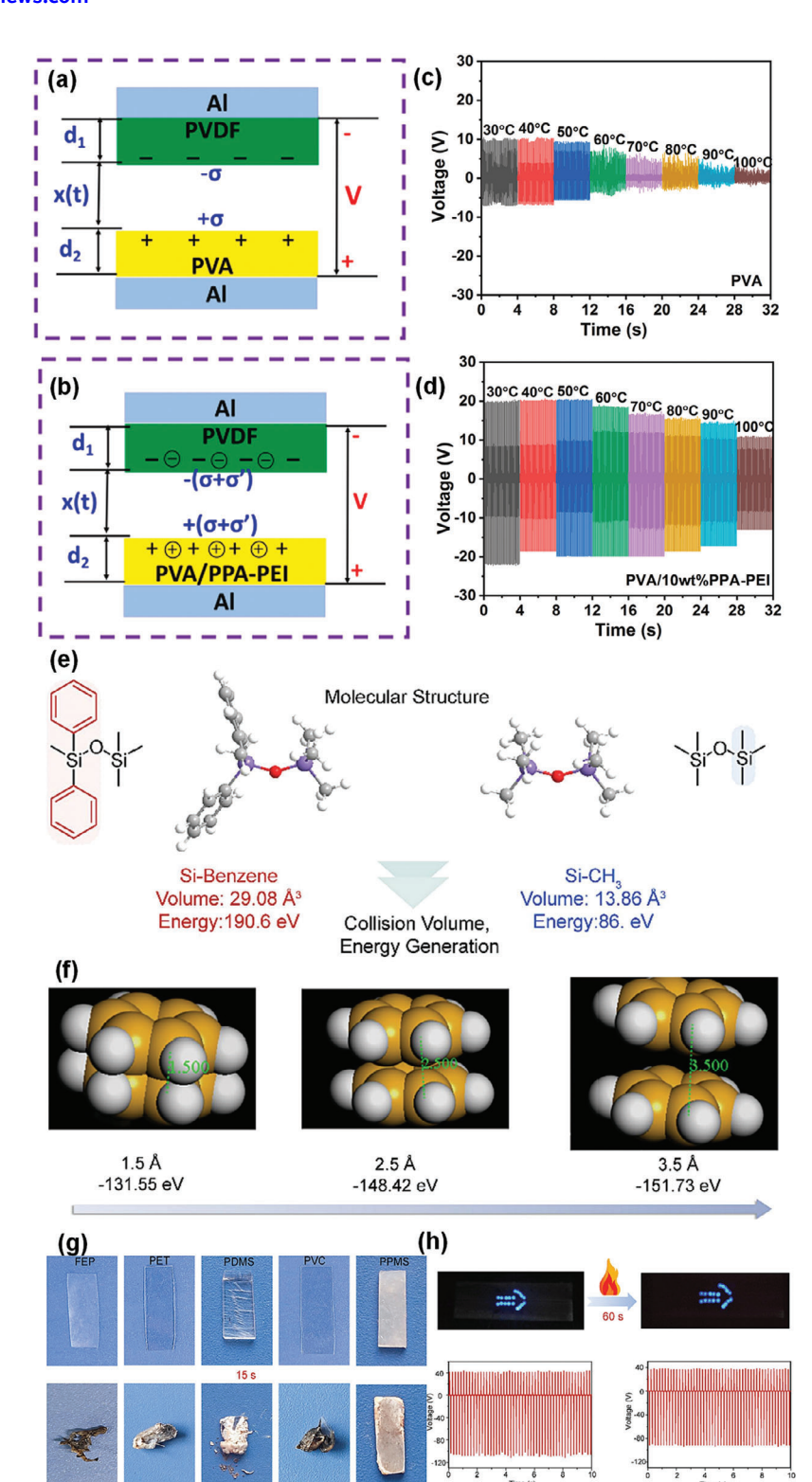


Figure 4. a) The charge transfer in pristine TENG during contact electrification is dominated by electron transfer. b) The charge transfer of PPA-PEI-based TENGs during contact electrification is a hybrid of electron and ion transfer due to the ionization of polyelectrolyte leading to an increase of the surface charge density. The effect of temperature on the output voltage. c) In-operando output voltage of pure PVA-based TENG triggered by DMA with increasing temperature. d) In-operando output voltage of PVA/10 wt.% PPA-PEI-based TENG triggered by DMA with increasing temperature. a–d) Reproduced with permission, [102] Copyright 2021, Elsevier. e) Simulation Results of energy and volume for Si-benzene and Si-CH₃. f) Diagram of energy variation of benzene with the increased distance. g) Images of different polymeric materials after 15 s combustion. h) Output voltage and photos showing the lighting arrow symbol consisted of blue LEDs before and after 60 s combustion. e–h) Reproduced with permission, [103] Copyright 2024, Elsevier.

15214095, 2025, 9, Downloaded from https://advanced.onlinelibrary.wiley.com/doi/10.1002/adma.202415099 by Dægu Gyeongbuk Institute Of, Wiley Online Library on [20.03/2025]. See the Terms

and-conditions) on Wiley Online Library for rules of use; OA articles are governed by the applicable Creative Commons License

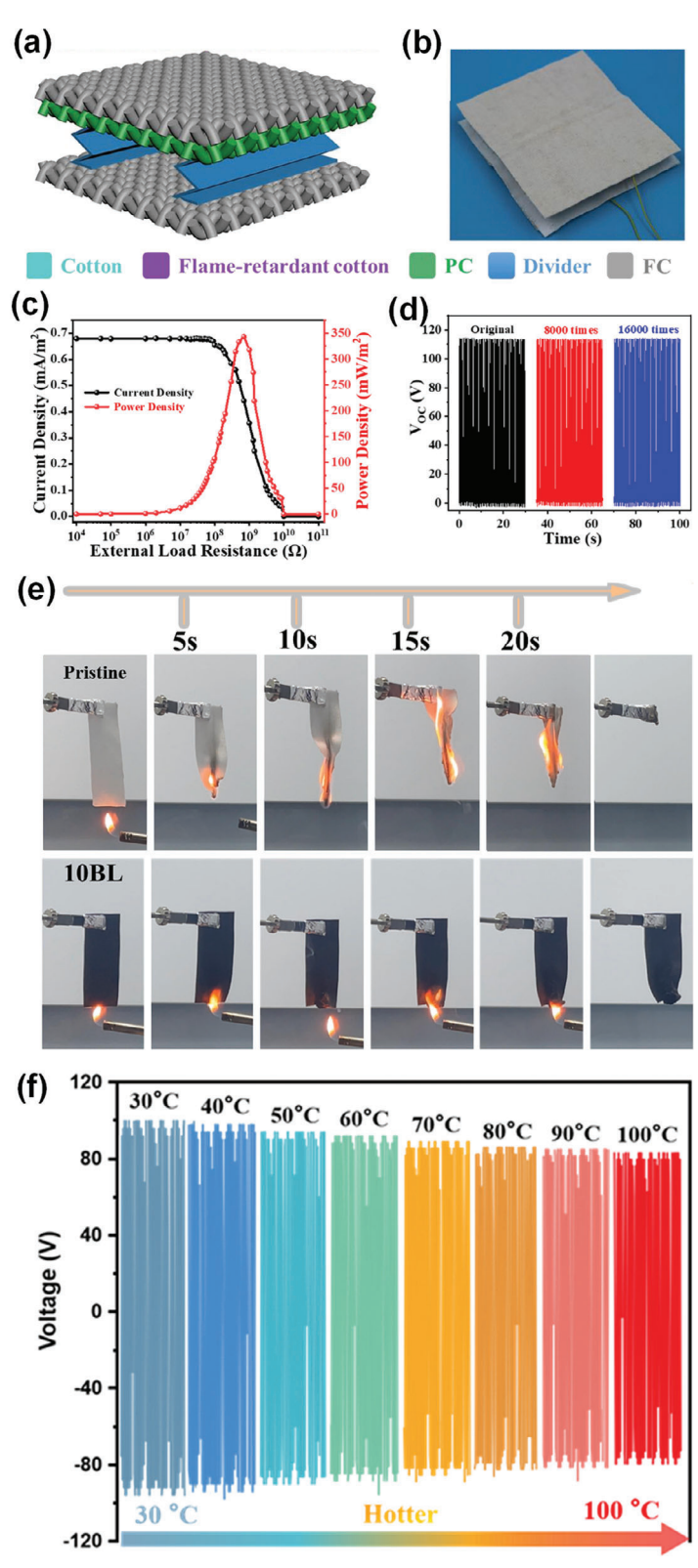


Figure 5. a,b) Schematic, photographic image of the FT-TENG. c) Variation of the output current density and power density with external resistances. d) Stability and robustness of FT-TENG. a–d) Reproduced with permission.^[104] Copyright 2020, American Chemical Society. e) Digital photos of 20 s combustion processes of pristine fabric and 10 BL coated NF. f) The voltage of treated NF-based TENG with increasing temperature (30–100 °C). e,f) Reproduced with permission.^[105] Copyright 2023, Elsevier.

www.advmat.de

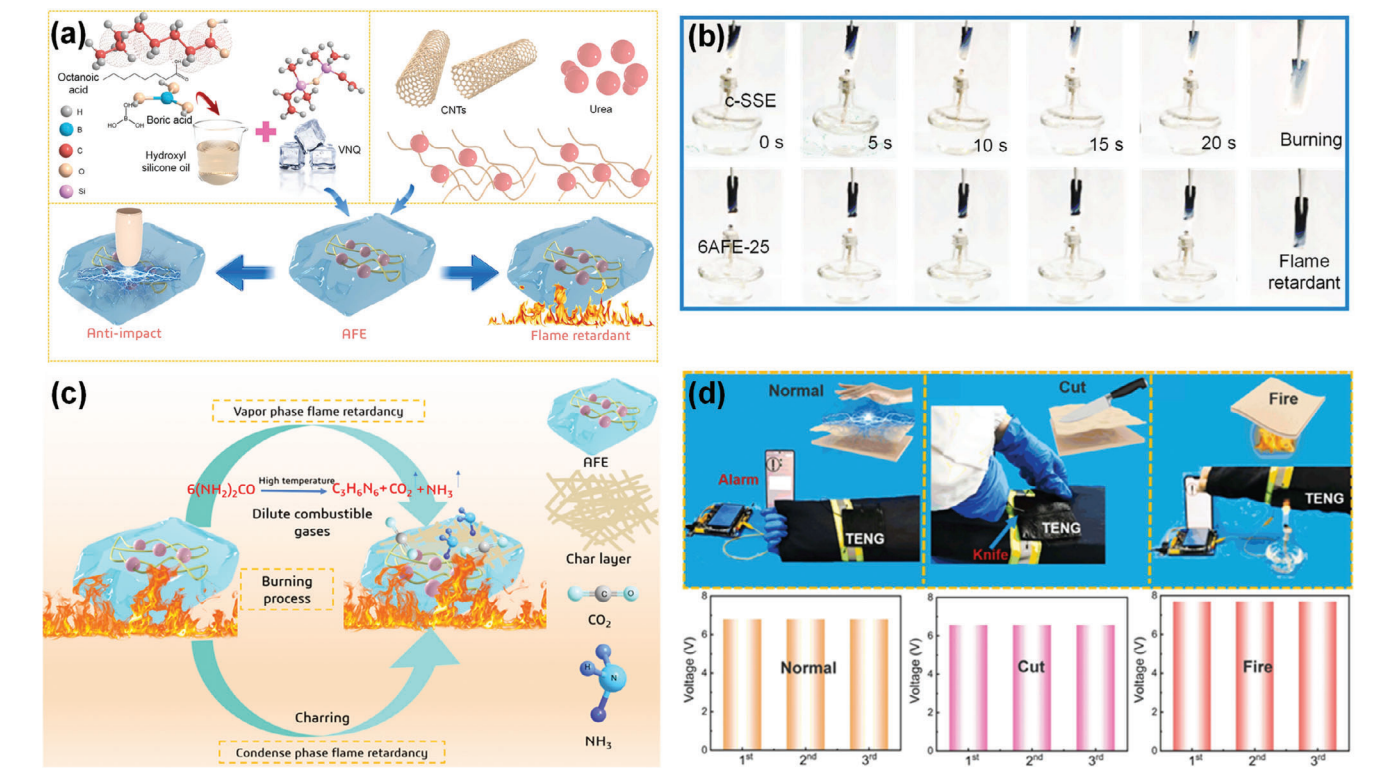


Figure 6. a) Schematic illustrating the fabrication process of the anti-impact and flame-retardant elastomers AFEs. b) Combustion experiments of c-SSE and 6AFE-25. c) Flame retardant mechanism for AFE composites. d) A diagram of the equipment could work under normal, cut-heal, and fire attack conditions and the corresponding electrical signals. a–d) Reproduced with permission. [108] Copyright 2022, Elsevier.

phytic acid solution using a layer-by-layer (LBL) self-assembly method, followed by coating it with silver. The PC was produced by soaking cotton fabric in the polytetrafluoroethylene solution. A PTFE film was chosen to act as a divider and was folded into a spring-like form. A vertical burning test was performed to assess the flame retardancy of the flame-retardant cotton fabrics. The heat release rate (HRR), total heat release rate (THRR), weight, and derivative weight of several specimens were determined. Furthermore, as the concentration or deposit times increased, the flame retardancy of the flame-retardant cotton fabrics was enhanced. The maximum power density of FT-TENG was 343.19 mW m⁻², corresponding to an external electrical load of 700 M Ω , as shown in Figure 5c. The stability of the device was tested for 16,000 cycles. From this study, there was no damage, and the output from the device is shown in Figure 5d. Even after being burned at 17 different spots, the FT-TENG retained 49.2% of its initial electrical output and when exposed to 220 °C, it similarly retained 34.48% of its electrical output. The FT-TENG was used as a wearable device for firefighters, functioning as a fire alarm system during forest fires.

Zhang et al. fabricated a flame-retardant conductive fabric-based TENG (FCF-TENG) using flame-retardant conductive nylon fabric (FC@NF) immersed in a mixture of chitosan-coated multi-walled carbon nanotubes (MWCNTs) and phytic acid (PA) solution produced by an LBL self-assembly method; the triboelectric cotton fabric (T@CF) was dipped in PTFE solution. [105] The vertical contact-separation mode-based TENG (dimensions: 5×5 cm²) achieved 85.2 V, $4.76~\mu\text{A}$, and $2.53~\mu\text{C}$. Unlike the pristine

nylon fabric, the 10 BL-FC@NF exhibited high flame-retardancy, and the specimen coated more than eight times did not catch fire after 20 seconds of ignition, as shown in Figure 5e. TGA showed that FC@NF has a smaller degradation rate than pristine nylon fabric. The voltage of the FCF-TENG at different temperatures (30–100 °C) is shown in Figure 5f. As temperature increases, voltage shows a decreasing trend, which can be explained by increased electron thermionic emission at higher temperatures, reducing the accumulation of surface charges on PTFE. Consequently, the findings demonstrate that the FCF-TENG has good thermal stability and maintains 90% harvesting efficiency, even at 100 °C. The authors utilized the properties of the FCF-TENG to fabricate a self-powered sensing system that transmits the electrical signals generated by individuals inside the building to the outside via Bluetooth to detect fire events remotely.

Chen et al. fabricated an anti-impact and flame-retardant elastomers (AFE)-based TENG. The 1 mm thick 1AFE-25 (containing 25% urea) with 3 mm thick 6AFE-25 (also containing 25% urea) layers are shown in **Figure 6a.**[106] A shear-stiffening elastomer (SSE) is soft but converts into a stiffer solid when subjected to dynamic impact, providing excellent kinetic energy dissipation properties. In addition, the SSE is self-healing, which can extend the life of the device. However, since the SSE is inherently combustible, the authors processed a conductive shear-stiffening elastomer (c-SSE) with excellent flame-retardant properties by blending it with carbon nanotubes (CNTs) and urea. A flexible AFE was fabricated by evenly mixing urea with the conductive shear-stiffening elastomer, whereby silicon hydroxide





www.advmat.de

oil, boric acid, octane, and CNT were utilized to form the c-SSE. The resulting contact-separation mode TENG, with dimensions of $60 \times 60 \times 4$ mm³ exhibited a maximum power of 57.25 uW at a voltage of 22.70 V. The voltage is improved from 7.49 to 22.70 V while increasing the external pressure from 6 to 30 N. The addition of urea enhanced the rheological properties of the composite. For example, with 25% and 30% urea, the G'max c-SSE was 0.24 and 0.27 MPa, contributing to improved triboelectric performance. Limiting oxygen index (LOI) and vertical combustion tests were conducted to assess the TENG's fire resistance. As shown in Figure 6b, pristine c-SSE ignited immediately upon contact with the flame. In contrast, the 6AFE-25 did not ignite fire for 20 s and maintained a stable electrical output. The 6AFE-25 reduced the PHRR by 29.10% compared to the SSE and received a V-0 rating with a higher LOI value (30.5%), indicating that the TENG has a high flame resistance. The flame-retardant mechanism is shown in Figure 6c. The authors successfully operated a Bluetooth alarm system to demonstrate the functionality of integrating this TENG into portable wearable devices and their electrical output in normal, cut, and fire conditions, as shown in Figure 6d.

5.2. Advanced Hybrid Composites

Qadeer et al. developed carbon fiber (CF)-reinforced liquid crystalline thermosetting (LCT) composites and utilized them to construct an FR-TENG.[107] The FR-TENG exhibited high flame resistance and good triboelectric performance, making it suitable for use in the drilling industry and extreme space regimes. The FR-TENG generated 125.7 V, 14 nC, and 0.8 µA, along with excellent thermal resistance. The majority of conventional triboelectric materials burned completely under comparable conditions; however, this fabricated FR-TENG remained combustible even after 60 s of burning. Furthermore, the authors demonstrated a carbon fiber-reinforced liquid crystalline thermosetting (LCT-2@BCF) composite having a shape memory effect (SME) and showcased its utilization as a fire alarm. Moreover, the improved Tg (≈270 °C), flexural strength, modulus (69.5 GPa), and ILSS (41.5 MPa) of LCT-2@ACF composites were influenced by surface treatments that enhanced interfacial contacts between fibers and resin matrices, leading to higher electrical output.

Guan et al. fabricated a fire-resistant TENG based on allaromatic liquid crystalline poly aryl ether ester (LCPAEE); the material was processed through a one-step melt polycondensation employing 4-hydroxybenzoic acid (HBA), 2,6-naphthalene dicarboxylic acid (NDA), and other materials. [108] Liquid crystalline polys (LCPs) were synthesized with HBA, BP, DHPE, TA, and NDA using typical melt condensation procedures, and the monomers were acetylated by boiling at 310 °C. Subsequently, volatiles were removed by cooling, resulting in a powder-like product. Thin films were processed using a melt pressing route with the powder being subjected to solid-state post-condensation. The flame initiation and combustion process decreased due to the LCPs, as shown in **Figure 7a**.

The mechanism of the flame-retardant property is illustrated in Figure 7b. When exposed to flames, LCPs demonstrate highly stiff chain stacking, effectively preventing heat transmission. The LCPs generate a small amount of carbon dioxide during degradation, diluting the oxygen concentration during burning, thereby reducing fire spread. This is because the unbroken surface of liquid crystalline polyaryl ether ester forms a barrier that insulates both heat and oxygen. The fabricated TENG maintained over 65% of its initial electrical output performance after being subjected to temperatures of 520 °C for 16 s, demonstrating long-term stability and reliability, as shown in Figure 7c,d. The experiment employed a straightforward synthesis technique known as one-pot multicomponent melt polycondensation. This method facilitates the use of inherently flame-retardant polymers and is expected to drive the development of future high-performance materials.

Qi et al. fabricated a flame-retardant TENG using PDMS and liquid metal (LM)/alginate composite fibers as triboelectric layers and aluminum foils as electrodes.[109] The authors used EGaIn with a Ga/In ratio of 75/25 wt./wt. in the manufacturing process of the LM/alginate composite filament. To stabilize a colloidal solution before undergoing the wet-spinning process, the sonication was employed to rupture LM droplets in the alginate solution of low concentration (0.5 wt.%), and the processed mixture was combined with an alginate solution of high concentration (6 wt.%). The flame-retardancy of the LM/alginate composite fibers was analyzed by limiting oxygen index (LOI), burning test, TGA, and microcalorimetry. The presence of LM droplets did not affect LOI. Unlike alginate fibers, during the burning tests, the LM/alginate fibers exhibited no smoldering and were extinguished immediately after the flame was removed. Scanning Electron Microscopy (SEM) images of the carbon residue after the micro-calorimetry test for alginate fibers and LM/alginate composites are shown in Figure 8a. A schematic of the flameretardant mechanism of LM/alginate composite fibers is shown in Figure 8b. Due to the high boiling point of LM, the shape of the LM/alginate fiber curve was similar to that of the alginate fiber curve, but the weight value was significantly higher. The heat release rate and total heat release of LM/alginate fibers were superior to those of alginate fibers. A vertical contact separation TENG generated a voltage of 198 V and a current density of 510 µA m⁻². The increased interfacial state density formed on the fiber surface leads to improved charge trapping capabilities and enhanced TENG performance of LM droplets (Figure 8c,d). However, TENG performance cannot be permanently improved by significantly higher LM content (>20 wt.%). This may be due to electrons hopping across the sites and creating a small space between the LM droplets on the fiber surface. The authors also emphasized the robust stability under harsh conditions and other properties that can be utilized in photothermal therapy and EMI shielding (Figure 8e,f).

Kim et al. designed a TENG device based on a thermal ion-gel-based conventional ionic liquid (IL) using 1-ethyl-3-methylimidazolium bis(trifluoromethyl sulfonyl)imide (EMIM-TFSI), a small number of lithium bis(trifluoromethyl sulfonyl)imide salt, and a plasticizer (tetraglyme) for ion transport, quick polarisation, transparency, flexibility, bi-continuous phase, and fire retardancy, as shown in **Figure 9a.**[110] To synthesize the ion-gel film, a PDMS stamping method using PDMS silicone elastomer-coated glass was employed. This approach prevented ion leakage and uneven film formation that typically occur with conventional spin-coating methods. The 20 wt.% ionic liquid (IL-TENG) device generated 150 V and 45 μA using a pushing force and a grounded structure to generate power from a single

15214095, 2025, 9, Downloaded from https://advanced.onlinelibrary.wiley.com/doi/10.1002/adma.202415099 by Dægu Gyeongbuk Institute Of, Wiley Online Library on [20.03/2025]. See the Terms

and-conditions) on Wiley Online Library for rules of use; OA articles are governed by the applicable Creative Commons License

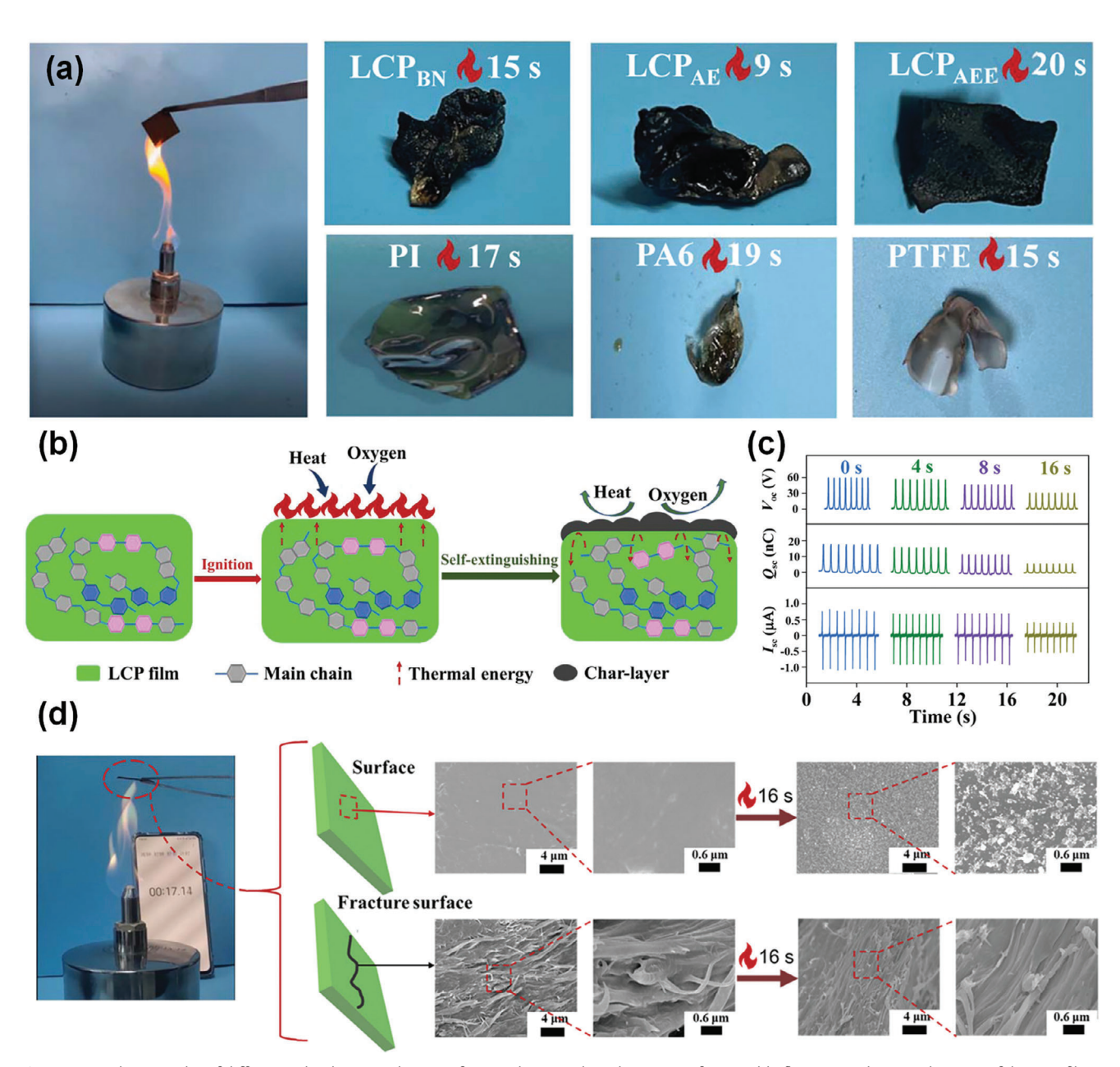


Figure 7. a) Photographs of different triboelectric polymers after combustion. b) Schematics of a possible flame-retardant mechanism of the LCP films. c) The electrical output performance of LCPAEE-TENG after burning 4, 8, and 16 s, respectively. d) SEM images of the surface and interior morphology of LCPAEE before and after 16 s combustion. a–d) Reproduced with permission. [108] Copyright 2022, Wiley.

TENG. The higher dipole moment generated by the ionic groups formed by TFSI anions, lithium cations, and EMIM cations essentially causes the dielectric constant to increase. This suggests that increasing the dielectric constant can improve the triboelectric performance and maximum charge density. Additionally, the TENG can withstand flames for 20 s, demonstrating superior heat resistance compared to conventional triboelectric materials. Ion-gel composite materials at various IL concentrations and their conductivities were compared. The results indicated in Figure 9b,c show that the TENG exhibited the highest power density of 300 μW cm⁻² at a concentration of 20 wt.%. The optimal conditions of ILs and the utilization of an Electric Double Layer can be factors for high-performance TENG. The device has successfully driven 50 green LEDs. This device exhibited stable output even after 500 cycles, demonstrating high durability.

Zhou et al. fabricated a flame-retardant and anti-dripping TENG using the excellent thermal characteristics of liquidcrystalline polyacrylate (LCP) copolymerized with PET. The LCP/PET was utilized as the triboelectric layer of a TENG with flame resistance.[111] An LCP based on 4-hydroxybenzoic acid (HBA), 4,4'-dihydroxybiphenyl (BP), 1,4-dicarboxybenzene (TA), and 2,6-naphthalene dicarboxylic acid (NDA) was copolymerized with PET using melt polycondensation, resulting in a high heat resistance, as shown in Figure 9d. Conventionally, flame

15214095, 2025, 9, Downloaded from https

library.wiley.com/doi/10.1002/adma.202415099 by Dægu Gyeongbuk Institute Of, Wiley Online Library on [20/03/2025]. See the Term

and-conditions) on Wiley Online Library for rules of use; OA articles are governed by the applicable Creative Commons

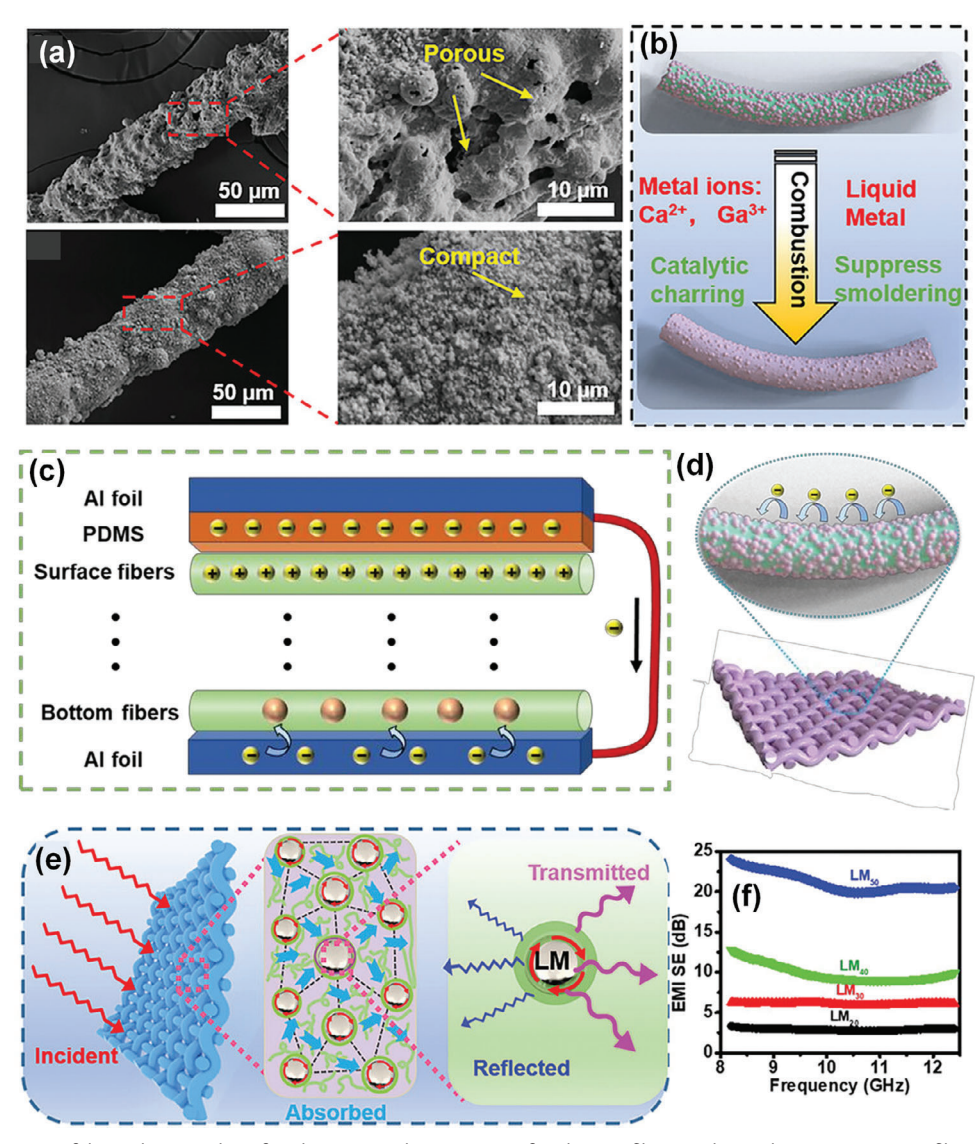


Figure 8. a) SEM images of the carbon residue after the micro-calorimetry test for alginate fibers and LM/alginate composite fibers. b) Flame retardant mechanism of LM/alginate composite fibers. c) Schematic diagram of charge trapping for LM particles. d) Schematic diagram of electrons hopping for LM/alginate composite fibers. e) EMI shielding mechanism of LM droplets in composite fibers, and f) EMI SET of LM/alginate fibers with various LM contents. a-f) Reproduced under the terms of the CC-BY Creative Commons Attribution 4.0 International license (https://creativecommons.org/ licenses/by/4.0). [109] Copyright 2023, the authors, published by Wiley-VCH.

retardancy was imparted to triboelectric materials by chemically bonding phosphorus to the main chain of PET. However, most phosphorus-containing PET materials tend to drip when exposed to fire, causing secondary damage. HBA exhibited excellent flame resistance and anti-dripping properties, providing greater stability than triboelectric materials. The FR-TENG exhibited an output of 60 V, 1.7 µA, and 17 nC, respectively. Unlike other materials, this TENG did not burn and maintained a stable output (32 V, 0.7 µA, 5 nC) even when exposed to combustion at 500 °C for 15 s. To evaluate the flame retardancy of the synthesized LCP/PET, microscale combustion calorimetry was employed. The PHRR of all LCP/PET samples remained below 200 W g⁻¹, indicative of the retarding effect of the LCP segment on flame ignition and combustion, as shown in Figure 9e. A dig-

ital image of LCP/PETs after combustion for 15 s is shown in Figure 9f.

Weldemhret et al. created high-carbon expandable graphite flakes (EGFs) and carbon black (CB) filler-loaded polyurethane foam (PUF) using an ionic liquid as a tertiary catalyst.[112] The thermal stability was evaluated using TGA in the N₂ atmosphere. The formulations for preparing different PUFs are shown in Table 1. Among them, PUF6 showed the best results from TGA compared to the other PUF formulations, especially the pristine PUF. The direct burning test and the UL-94 vertical burning test, shown in Figure 10a, indicated better flame-retardancy of PUF6 and PUF8. High carbon sponge fillers generated by this fabrication method prevented melt spillage when ignited by a butane torch (≈1400 °C, applied for 20 s) and self-extinguishing

15214095, 2025, 9, Downloaded from https://advanced.onlinelibrary.wiley.com/doi/10.1002/adma.202415099 by Dægu Gyeongbuk Institute Of, Wiley Online Library on [20.03/2025]. See the Terms and Conditions (https://onlinelibrary.wiley.com/terms

and-conditions) on Wiley Online Library for rules of use; OA articles are governed by the applicable Creative Commons License

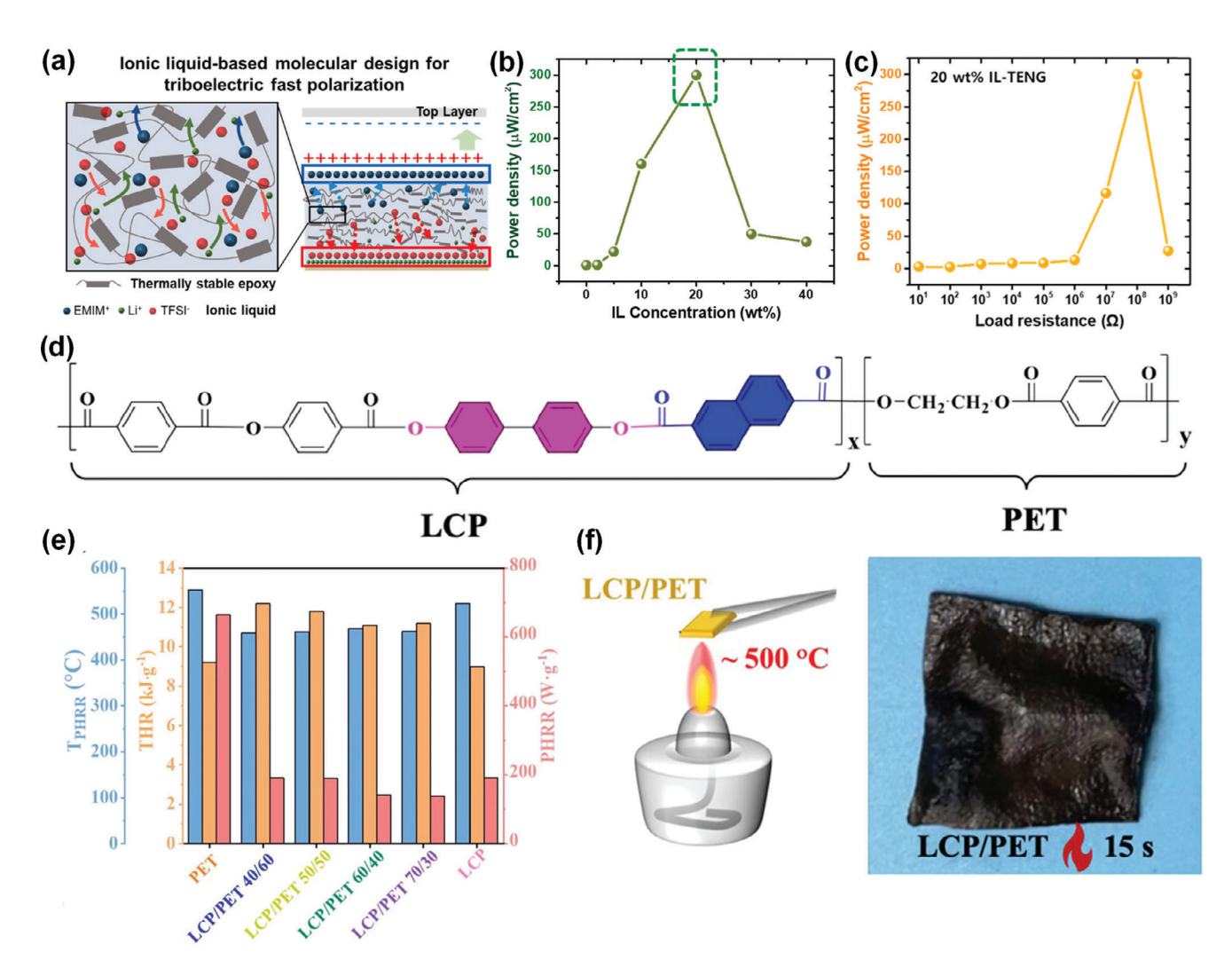


Figure 9. a) Schematic of ion-gel-based triboelectric layer for ion transporting, fast polarization, transparency, flexibility, bi-continuous phase, and fire retardancy. b) The power density of TENG with different IL concentrations (0–40 wt.%). c) The power density of the 20 wt.% IL-TENG with the resistance of external loads up to $10^9~\Omega$. a–c) Reproduced with permission. [110] Copyright 2021, Elsevier. d) Copolymerization of LCP with PET via melt polycondensation e) PHRR test of all samples. f) Digital images of LCP/PETs after combustion for 15 s. d–f) Reproduced with permission. [111] Copyright 2022, American Chemical Society.

Table 1. Formulations for preparing flexible polyurethane foam.

Sample	Polyol (g)	H ₂ O [g]	IL [g]	CB [g]	EGFs [g]	MDI [g]
PUF1	100	1.0	/	/	/	36
PUF2	100	1.0	10	/	/	36
PUF3	100	1.0	10	5.0	35	36
PUF4	100	1.0	/	/	/	50
PUF5	100	1.0	10	/	1	50
PUF6	100	1.0	10	5.0	35	50
PUF7	100	1.0	10	5.0	/	50
PUF8	100	1.0	10	/	35	50
PUF9	100	1.0	/	5.0	35	50

15214095, 2025, 9, Downloaded from https://adv.

onlinelibrary.wiley.com/doi/10.1002/adma.202415099 by Dægu Gyeongbuk Institute Of, Wiley Online Library on [20.03/2025]. See the Terms

onditions) on Wiley Online Library for rules of use; OA articles are governed by the applicable Creative Commons License

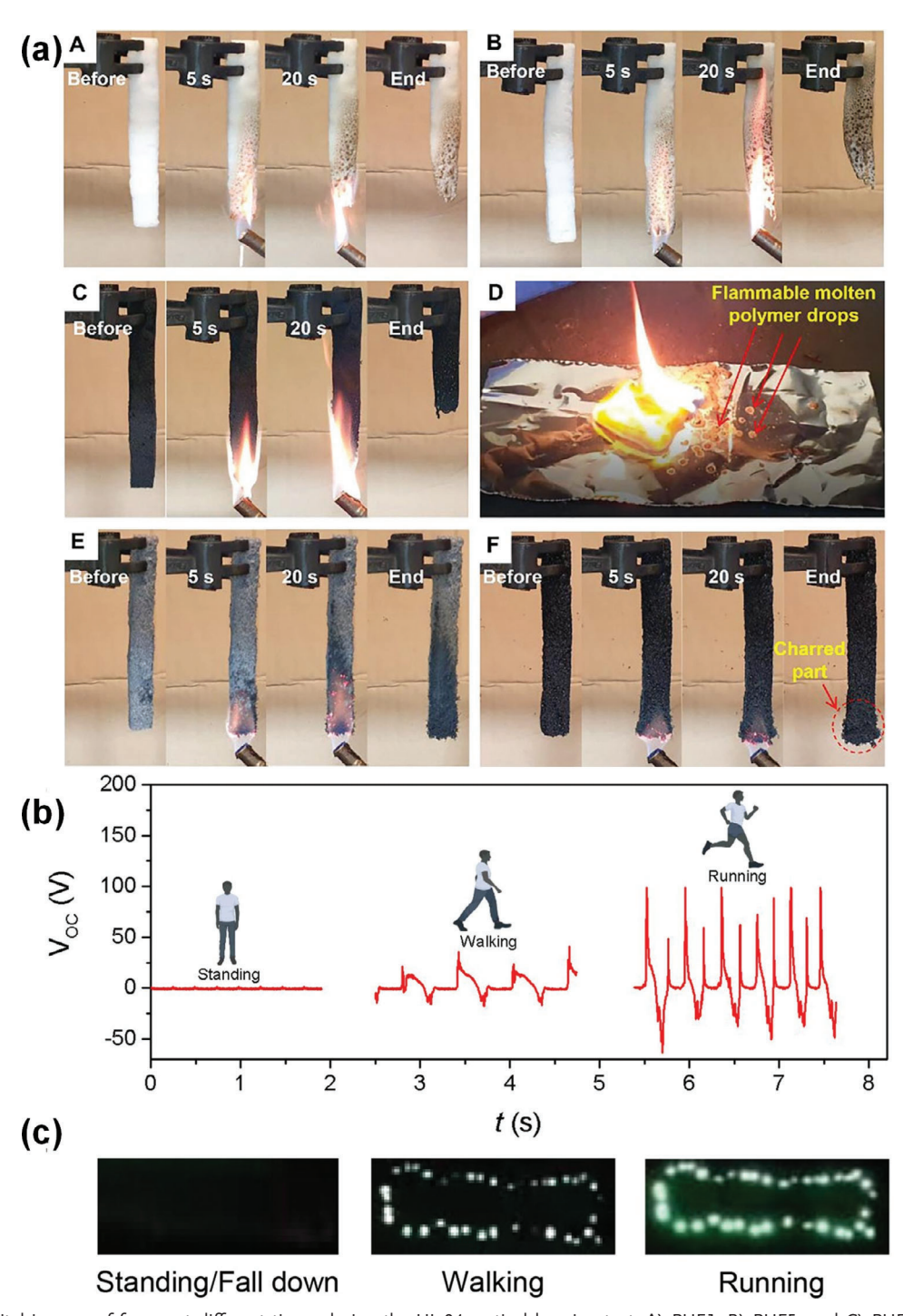


Figure 10. a) Digital images of foams at different times during the UL-94 vertical burning test. A) PUF1, B) PUF5, and C) PUF7 burn rapidly and D) generate flammable molten polymer that is capable of transferring fire to a material underneath. E) PUF8 and F) PUF6 show excellent flame resistance. b) Biochemical energy harvesting using FR-TENG attached under a shoe sole. c) Glowing 38 green LEDs using FR-TENG attached under a shoe sole. a–c) Reproduced with permission.^[113] Copyright 2022, Elsevier.

after torch removal, preventing foam collapse, and demonstrating exceptional flame retardancy. In addition, the key flame retardancy metrics peak heat release rate, total heat release, and total smoke release were reduced by 73%, 78%, and 92%, respectively, and were able to meet the UL-94 V-0 standard. The

authors fabricated a single-electrode FR-TENG with PUF6 as a tribopositive layer and PTFE as a tribonegative layer. The voltage and current increased to 130.6 V and 15.6 μ A cm $^{-2}$ for PUF6, 35.0 V and 7.6 μ A cm $^{-2}$ for PUF7, and 58.7 V and 12.5 μ A cm $^{-2}$ for PUF8, respectively. It can be seen that adding carbon fillers,

and-conditions) on Wiley Online Library for rules of use; OA articles are governed by the applicable Creative Commons License

www.advmat.de

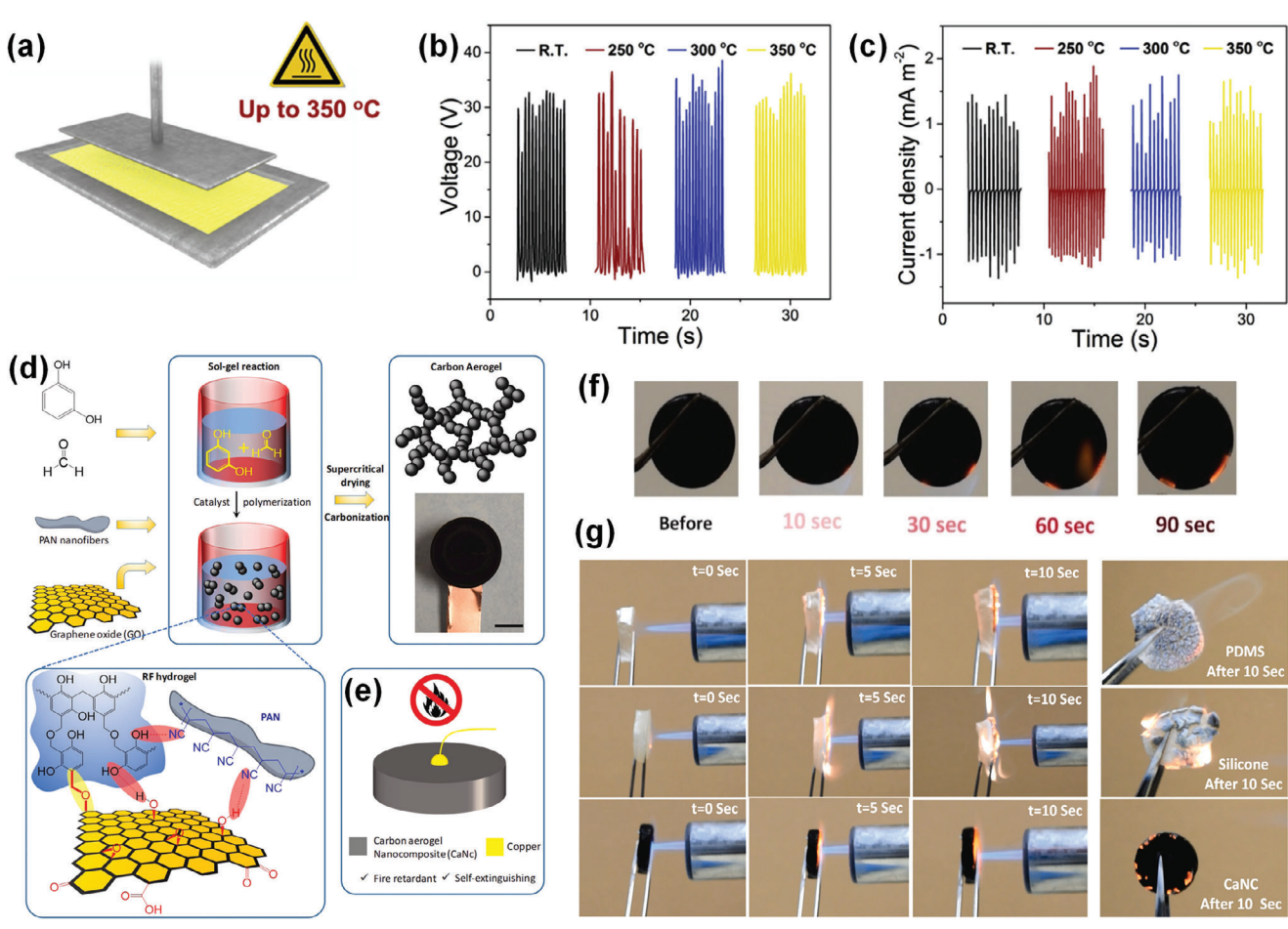


Figure 11. a) Schematic of PBOA/Al TENGs. An aluminum plate is hung over the PBOA film marked in yellow. b) Open-circuit voltage and c) Current density of PBOA/Al TENGs performed under different temperatures. a–c) Reproduced with permission. [113] Copyright 2019, Elsevier. d) Fabrication steps of FR-TENG containing a hybrid carbon aerogel with functionalized nanofibers/nanosheets. e) Schematic of a single-electrode mode of FR-TENG. f) FR-TENG vertical burning test before the test, after 90 s of application of a butane flame, showed super high flame resistance. g) Photographs showing the torch burn test for the following samples: (first row) PDMS, (second row) silicone, and (third row) CaNC (The samples are ignited using a butane burner, then exposed to the flame for 10 s). d–g) Reproduced with permission. [114] Copyright 2019, Elsevier.

particularly 3D stacked EGF sheets, and 0D spherical CB particles, helped improve the foam composite's TENG performance. The authors affixed the FR-TENG under a shoe sole and measured open-circuit voltage in standing, walking, and running situations. The differences in electrical output could be visually confirmed by comparing images of lighting 38 LEDs as shown in Figure 10b.c.

5.3. Aerogels

Qian et al. fabricated a FR-TENG using polyethylene oxide (PEO) film for positive tribo-materials and poly p-phenylene benzo-bisoxazole aerogels (PBOAs) film for negative tribo-materials. [113] The PBOA was paired with an aluminum foil to fabricate a TENG. The decomposition temperature of PBOA is 650 °C, making it ideal for high-heat applications. The TENG was able to produce an electrical output at 350 °C, and the increased temperature did not affect the TENG performance, as seen in Figure 11a–c. They experimented with the performance of

PBOA/PEO TENGs and compared the gap distance between PBOA and PEO films, impact force, and frequency. The V_{OC} was 40, 35, and 24 V when the thicknesses of the PBOA film were 30, 45, and 60 μ m, respectively. The J_{SC} reached 1.4 mAm $^{-2}$ and then decreased with increasing thickness of the PBOA film. The charge densities were 32, 28, and 20 μ Cm⁻². The V_{OC} and J_{SC} increased from 32 V to 40 V, 1.1 and 1.4 mAm⁻², respectively, as the distance between films increases from 1 to 3 mm. As the impact force increased from 1 to 5N, the $V_{\it OC}$ reached from 8.4 to 33 V, and the J_{SC} reached 1.0, 1.1, 2.9, and 2.9 mAm⁻² corresponding to the impact forces of 1, 5, 10, and 20 N, respectively. They achieved a V_{OC} of 40 V, J_{SC} of 2.9 mAm⁻² and a charge density of 722.9 µCm⁻² respectively. Due to the high specific surface area and significant porosity of PBOA, the resulting TENGs also exhibited high performance. The device could light up 36 LED bulbs and charge a capacitor to 10 V within 250 s; the maximum power density was 28 mWm⁻² was obtained at the resistance of 50 M Ω when the resistance was connected to an external load after optimizing the parameters of PBOA/PEO TENGs. PBOA rapidly carbonized when exposed to a flame at 1000 °C



www.advmat.de

and instantly self-extinguished after the igniter was removed. The PBOA/Al TENGs exhibited a $V_{\rm OC}$ of 32 V, a J_{SC} of 1.2 mA m^{-2} , and a charge density of 32 μC m^{-2} at a temperature as high as 350 °C.

Ahmed et al. developed a flame-retardant and selfextinguishing TENG using carbon aerogel (CaNC) generated from sol-gel polymerization of resorcinol and formaldehyde, as illustrated in Figure 11d.[114] The FR-TENG utilizes the outstanding thermal properties of carbon derived from a resorcinol-formaldehyde aerogel, with enhancements in its electrical, mechanical, and triboelectric properties achieved through the introduction of polyacrylonitrile nanofibers and graphene oxide nanosheets, which have a higher specific surface area and enhanced charge transfer rate. As shown in Figure 11e, a single-electrode mode of FR-TENG was employed to achieve a high electrical output of 80 V and 25 µA m⁻² current through repeated cycles of pressing and releasing fluorinated ethylene propylene (FEP) on CANC directly. The FR-TENG effectively charged a 1 µF capacitor from 0 to 6 V in ≈5 min through standard pressing at a frequency of 3 Hz. After exposure to acetone flames to test the flame resistance of the FR-TENG, it maintained stable electrical output after 90 s of exposure to flames.

Furthermore, it was able to operate reliably up at temperatures to 200 $^{\circ}$ C, with a decrease in voltage observed at higher temperatures. This CaNC self-extinguished within 10 s after removing the flame source, and the performance of the sample is preserved after that (Figure 11f,g). Thus, the FR-TENG provides a safe alternative material for consumer products capable of preventing and extinguishing fires. The FRTENG, made from a non-flammable nanocomposite without harmful substances, and stands out as an environmentally friendly solution.

Hu et al. designed high-temperature resistant silicon aerogel and fiber feeling-based TENG (HTFs-TENG) by employing a flexible high-temperature resistant substrate made of silicon aerogels (SAG) and needled felt (NF).[115] The process involved needle-punching a blend of pre-oxidized polyacrylonitrile (OXPAN) and polyphenylene sulfide (PPS) fibers to create a flexible needled felt (NF), which was then combined with SAG. Following hydrophobic modification, the HTFs-TENG was encapsulated in silica gel. To enhance the electrical performance of the HTFs-TENG, barium titanate (BT) particles, known for their high relative permittivity and low dielectric loss, were incorporated into the SAG. The BT-modified high-temperature fiber substrates were designated as 10 g L⁻¹-BT-SAG/NF, 20 g L⁻¹-BT-SAG/NF, and 30 g L⁻¹-BT-SAG/NF. While the SAG composite felt without BT particles withstood a butane flame at temperatures up to 1300 °C for ≈4 min, the 30 g L⁻¹-BT-SAG/NF composite resisted the flame for over 10 min. The HTFs-TENG demonstrated functionality across a wide temperature range, operating effectively between -75 and 275 °C. At room temperature (25 °C), it achieved a peak voltage and current output of 135 V and 6 µA, respectively, along with an instantaneous power density of 31.9 mW m⁻² when paired with a load resistance of 100 M Ω . This approach successfully tunes the dielectric properties to enhance the electrical performance of HTFs-TENGs. Additionally, the device exhibited a responsive electrical signal under varying temperatures and frequencies, even at extremely low frequencies below 1 Hz.

5.4. Biomaterials

Luo et al. fabricated a flame-retardant wood-based TENG using a straightforward three-step method involving basswood and various chemicals.[116] Chemical treatments for flame-retardant wood are crucial for enhancing the mechanical and flameretardant properties of wood. This modification results in thicker and rougher cell walls, as illustrated in Figure 12a,b. The strong flame-retardant wood was produced by hot-pressing bentoniteinfiltrated wood, which was then employed in the construction of the TENG. The mechanical properties of the treated wood surpass those of natural wood. A commercial PTFE film was used as a moving object to assess the TENG's electrical output, achieving a power density of 24.2 mW m⁻² at 50 M Ω . The electrical output performance of TENGs based on natural wood and flame-retardant wood is nearly identical; however, the flame-retardant wood-based TENG retained 68% of its electrical output even after 60 s of exposure to 250 °C (Figure 12c-d), while the standard wood-based TENG was destroyed before generating any electric power. The electrical output after different combustion experiments is shown in Figure 12e-g. Compared to normal wood, the flame-retardant wood had a 7.7-fold increase in strength, a 32% reduction in peak heat release rate, and the ability to self-extinguish. The flame-retardant wood-based TENG was employed to design a self-powered tactile sensor for intelligent wireless fire monitoring. This TENG, which harvests energy from human walking and running, was effectively integrated into the fire evacuation system.

Wang et al. used biocompatible black phosphorus (BP) and phytic acid (PA) flame-retardants to design a single-electrode cellulose-based TENG.[117] The CNF-BP-PA film and Ag layer served as the triboelectric layer for the FR-TENG. The CNF-BP-PA film was rendered fire-retardant by incorporating BP and PA into CNF via a vacuum filtering method, as seen in Figure 13a. This combination resulted in the FR-TENG exhibiting excellent biocompatibility and the ability to decompose in soil. The FR-TENG demonstrated an output of 116 V and 3.02 mA m⁻² at 2 Hz, successfully charging commercial capacitors within 160 s. Microscale combustion calorimeter (MCC) test results indicated that the CNF-BP-PA/AgNWs film possesses superior fire resistance and flame retardancy compared to pure CNF film, with reductions in PHRR and HRR of 64.6% and 47.6%, respectively. Additionally, the LOI was raised to 39.1%. The flameretardant mechanism illustration of CNF-BP-PA film is shown in Figure 13b. Furthermore, the FR-TENG exhibited a strong response to temperature and humidity, with values of 3779.16 K and 1.436 V/% relative humidity (RH), respectively. This capability enables the FR-TENG to provide precise monitoring and prompt warnings for fires and elevated temperature conditions, responding rapidly within a 5 s timeframe, as presented in Figure 13c. In the temperature range of 35–150 °C, the fabricated FR-TENG demonstrated a high thermal index of 3779.16 K.

Zhang et al. developed a flame-retardant hydrophobic fabric-based TENG (FHF-TENG) using flame-retardant hydrophobic coated nylon fabric (FH@NF) and PTFE-coated cotton fabric (P@CF). The FH@NF was prepared by immersing nylon fabric in a chitosan solution containing aminated MWCNTs and hydrophobic silica nanoparticles, followed by dipping in a phytic

15214095, 2025, 9, Downloaded from https://advanced.

onlinelibrary.wiley.com/doi/10.1002/adma.202415099 by Dægu Gyeongbuk Institute Of, Wiley Online Library on [20.03/2025]. See the Terms

onditions) on Wiley Online Library for rules of use; OA articles are governed by the applicable Creative Commons License

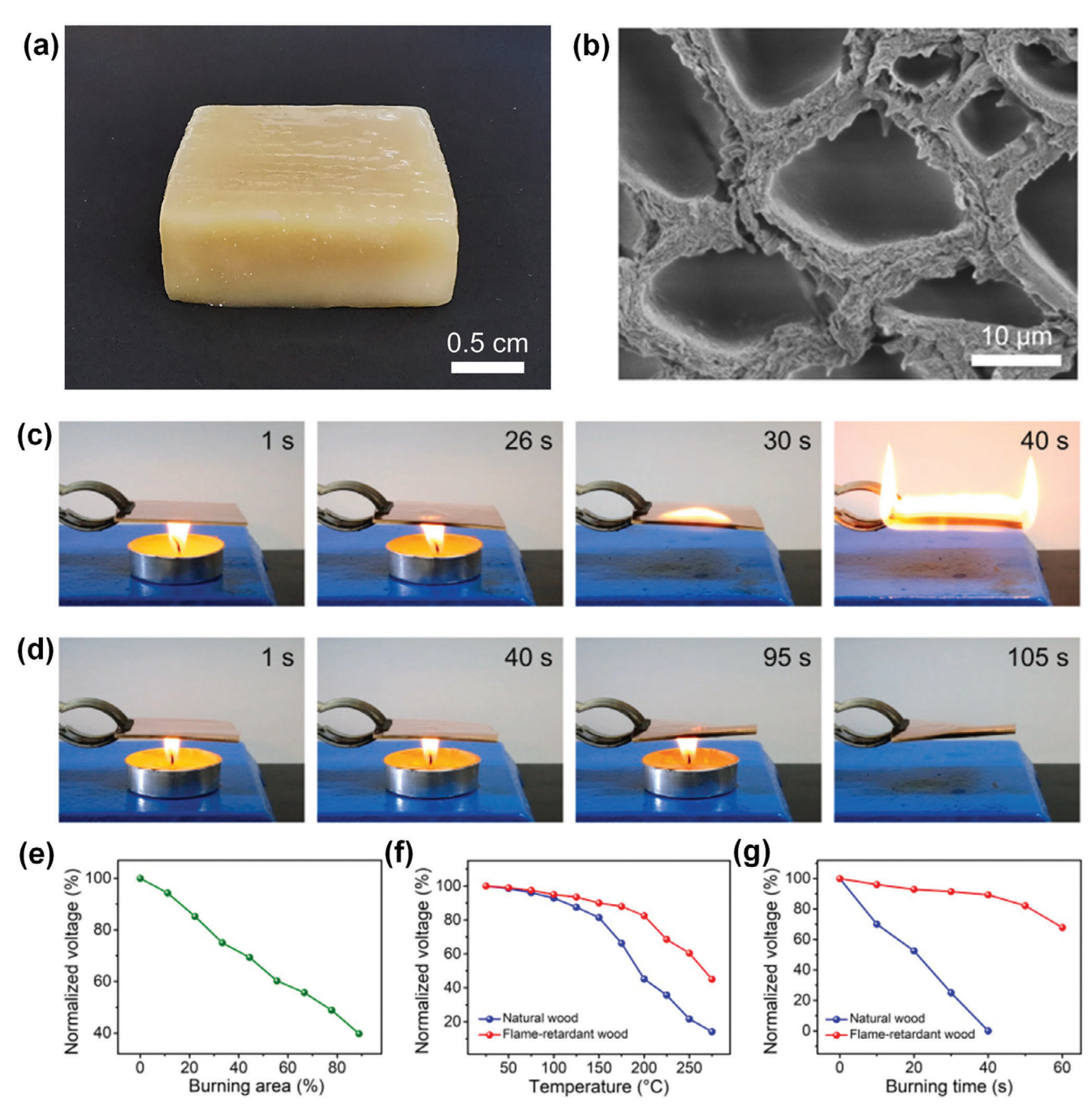


Figure 12. a,b) Digital image and cross-sectional SEM image of flame-retardant wood. Photographs showing the combustion process of the TENG fabricated with natural wood c) and flame-retardant wood d). e) Normalized voltage of the FW-TENG after burning different areas. f) Normalized voltage of the TENGs fabricated with natural wood and flame-retardant wood under different temperatures. g) Normalized voltage of the TENGs fabricated with natural wood and flame-retardant wood under different burning times. a-g) Reproduced with permission.[116] Copyright 2022, Elsevier.

acid solution using the LBL method. The P@CF was developed by soaking cotton fabric in a PTFE solution. In direct ignition tests, the nylon fabric became increasingly difficult to ignite as the number of bi-layers (BL) increased. The TGA results indicated that, although the treated nylon fabric began to lose weight earlier than the pristine nylon fabric, the FH@NF retained more residual mass and exhibited a lower decomposition rate. During MCC tests, the FH@NF outperformed the pristine nylon fabric. The flame-retardant mechanism is shown in Figure 14a. The authors used PET films as substrates for FH@NF and P@CF to fabricate the FHF-TENG. To measure electrical output, a 5 × 5 cm² specimen with a 3 cm spacing and linear motion at 3 Hz was employed, with the outputs displayed in Figure 14b,c. This TENG demonstrates excellent flameretardant characteristics (self-extinguishment and melt-dripping resistance) and high energy harvesting efficiency, achieving a

15214095, 2025, 9, Downloaded from https://advanced.

onlinelibrary.wiley.com/doi/10.1002/adma.202415099 by Dægu Gyeongbuk Institute Of, Wiley Online Library on [20.03/2025]. See the Terms

onditions) on Wiley Online Library for rules of use; OA articles are governed by the applicable Creative Commons License

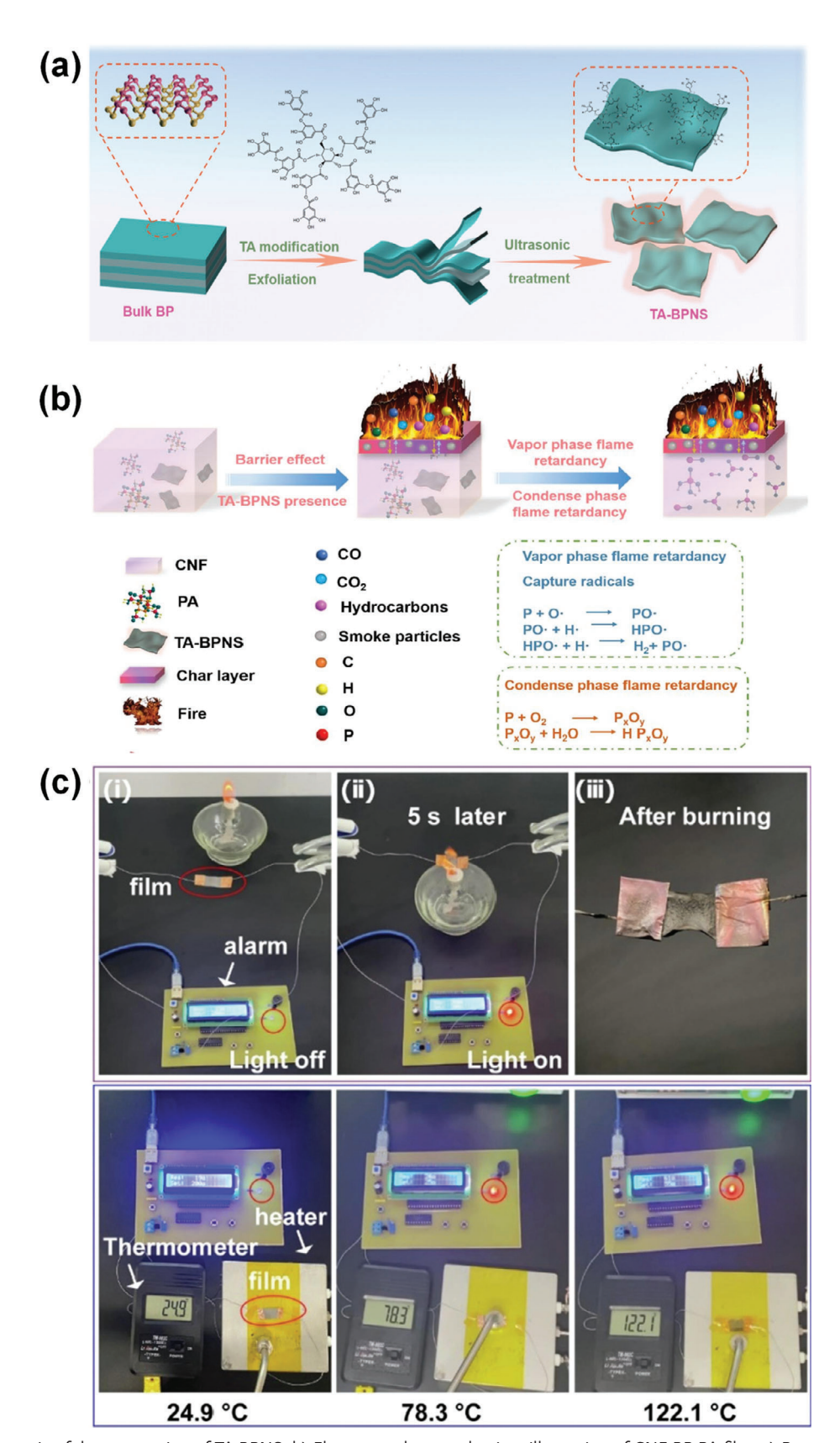


Figure 13. a) Schematic of the preparation of TA-BPNS. b) Flame-retardant mechanism illustration of CNF-BP-PA film. c) Process of FR-TENG flame detection and alarm system. Process of FR-TENG temperature detection alarm system. a–c) Reproduced with permission. [117] Copyright 2022, Elsevier.

www.advmat.de

15214095, 2025, 9, Downloaded from https:

onlinelibrary.wiley.com/doi/10.1002/adma.202415099 by Dægu Gyeongbuk Institute Of, Wiley Online Library on [20/03/2025]. See the Terms

onditions) on Wiley Online Library for rules of use; OA articles are governed by the applicable Creative Commons

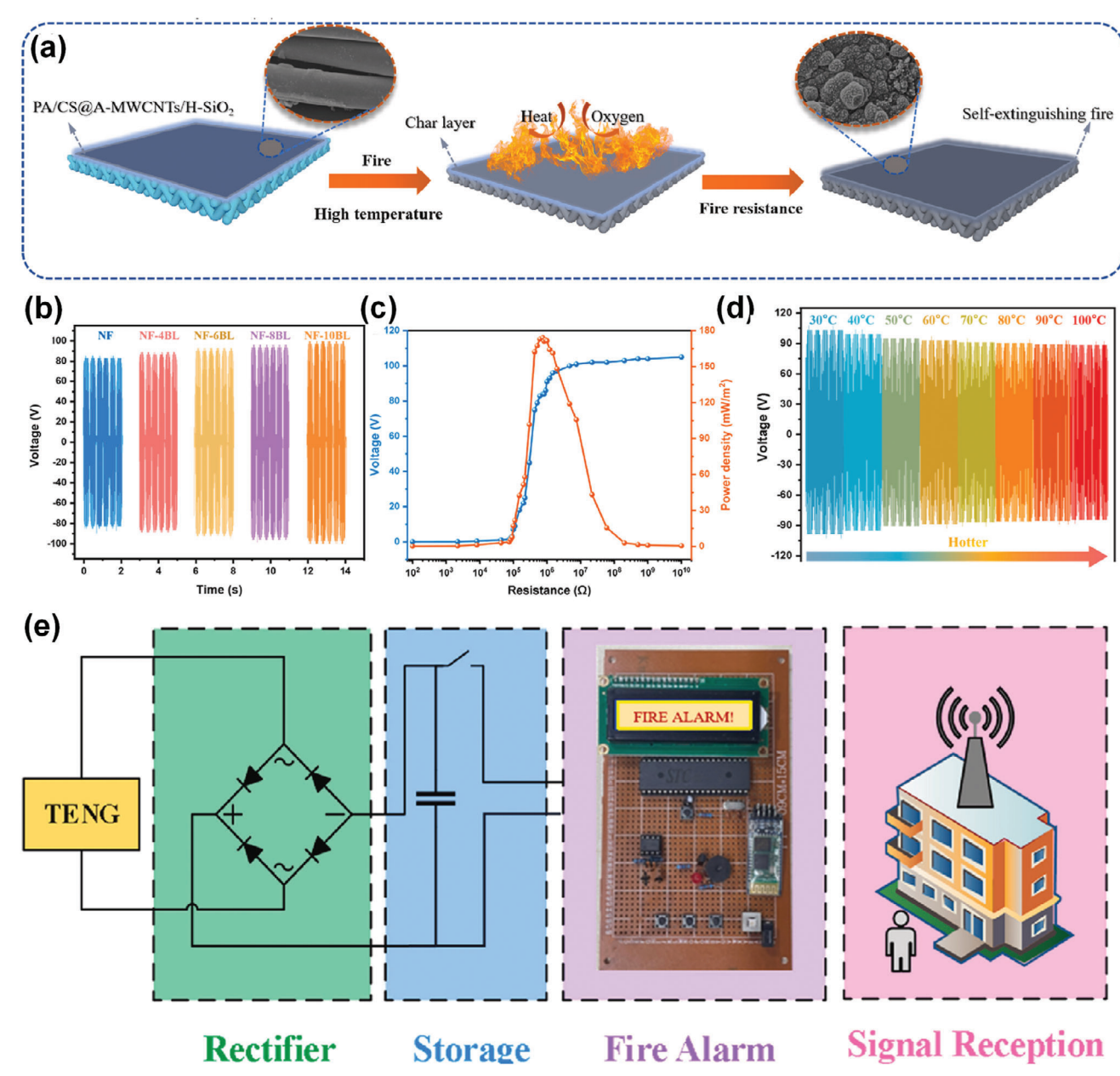


Figure 14. a) Flame-retardant mechanism of the fabric after exposure to flame. b) V_{oc} curves of NF with different coating layers. c) The voltage and power density of the FHF-TENG with a variation of external loading resistances ($10^2-10^{10}~\Omega$). d) The V_{oc} of the FHF-TENG with increasing temperature (30–100 °C). e) Diagram of the self-powered intelligent wireless fire-monitoring system. e–g) Reproduced with permission. [118] Copyright 2024, Elsevier.

peak output power of 173 mW m $^{-2}$. This demonstrates the effect of self-assembled layers (2–10 BL) of FH@NF on output power. This enhancement can be attributed to the ability of aminated MWCNT to establish a conductive network on the FH@NF. The voltage output of the FHF-TENG with increasing temperature (30–100 °C) is shown in Figure 14d. The resulting fire-monitoring system using the FHF-TENG is illustrated in Figure 14(e).

Similarly, Tang et al. developed a wood-based TENG (FW-TENG) with exceptional fire safety and electrical performance. Polyethyleneimine (PEI), a highly polar polycationic polymer with numerous amine groups, was employed

as a triboelectric filler for delignified wood. Its high nitrogen (N) content can interact with the phosphorus (P) element from flame retardants to enhance fire safety properties through a synergistic P-N effect. In this mechanism, phosphorous contributes to the formation of a stable phosphorus-containing carbon layer in the condensed phase, while nitrogen generates non-flammable gases at elevated temperatures, effectively diluting the concentration of flammable gases. The FW-TENG produced 198 V, 7.48 μA , and a maximum output power density of 119.7 mW m $^{-2}$. The surface potential values for flame-retardant and normal wood were found to be 0.496 and 0.461 mV, respectively suggesting that flame-retardant wood has a lower work function. This

www.advmat.de

15214095, 2025, 9, Downloaded from https://advan

onlinelibrary.wiley.com/doi/10.1002/adma.202415099 by Dægu Gyeongbuk Institute Of, Wiley Online Library on [20.03/2025]. See the Terms

and-conditions) on Wiley Online Library for rules of use; OA articles are governed by the applicable Creative Commons

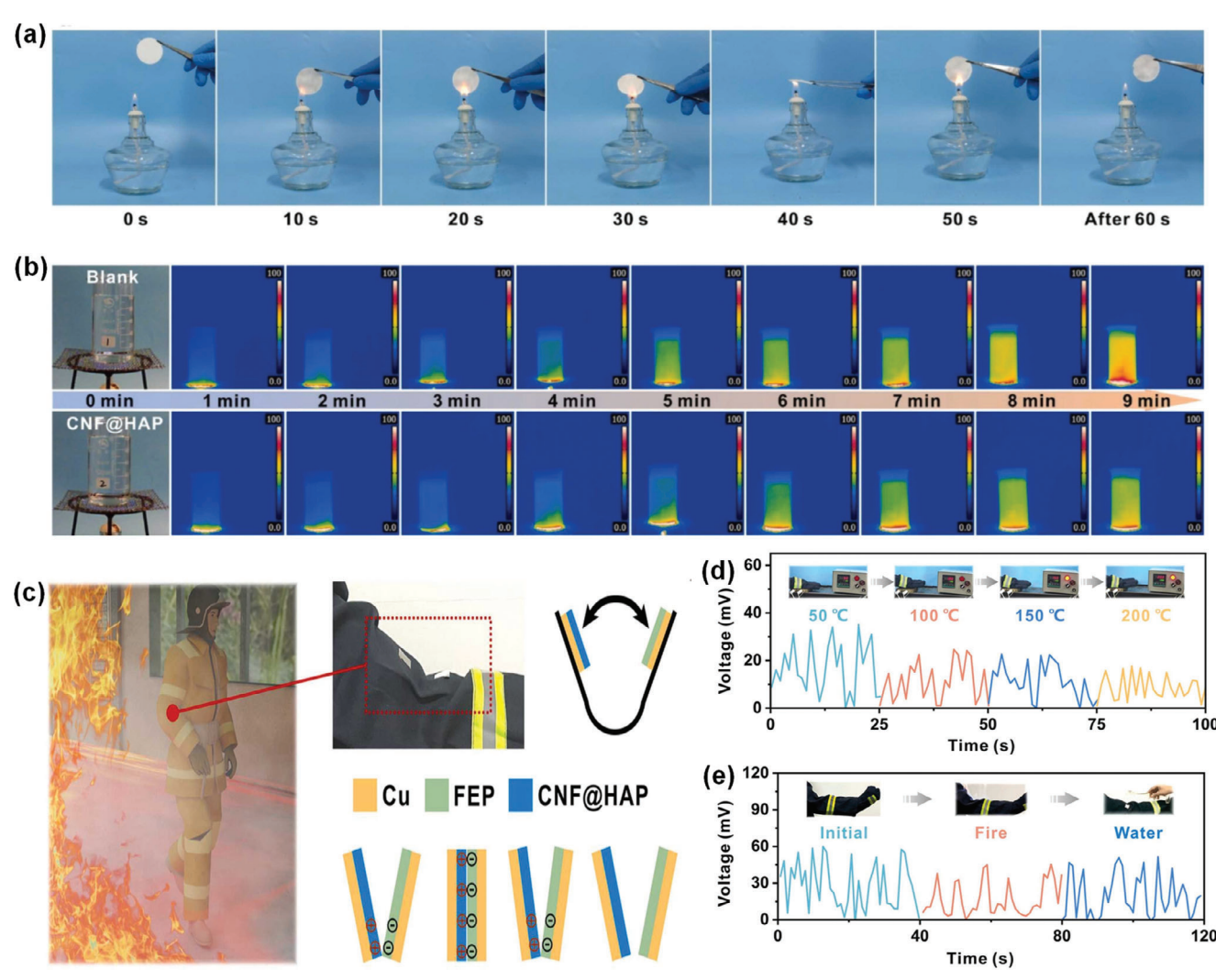


Figure 15. a) Changes of CH-12 composite films during combustion. b) Thermal insulation performance of CH-12 composite film. c) Schematic of the self-powered sensor installed at the elbow joint and the operating mode of the self-powered out sensor. d) Radio signal of single-electrode self-powered sensor at different temperatures. e) Radio signal of single-electrode self-powered sensor after receiving flame and water erosion. a—e) Reproduced with permission. [120] Copyright 2023, Elsevier.

characteristic increases the likelihood of electron transfer when the flame-retardant wood contacts the FEP surface, enhancing the surface charge density. Consequently, the addition of PEI, rather than surface roughness, is responsible for the improved triboelectric properties. Furthermore, it exhibits self-extinguishing activity upon ignition. Remarkably, even after ignition, the system can still operate with a response time of 260 ms. Before burning, the FW-TENG could generate an output voltage of $\approx\!1.0$ V, and after burning for 50 s, it can still produce more than 0.5 V. These findings suggest that the self-powered wireless fire monitoring system based on the FW-TENG enhances the rescue of trapped individuals in emergencies.

Duan et al. developed a flame-retardant cellulose nanofibril and hydroxyapatite (CNF@HAP) composite filament using a solvothermal method for HAP nanowires and a grafting method to attach the HAP to CNF by isophorone diisocyanate. [120] The TENG was fabricated using the CNF@HAP fiber as a tribopositive layer and ethylene FEP as a tribonegative layer. TGA tests of

the CNF@HAP film demonstrated improved flame-retardancy with an increasing ratio of HAP. Additionally, vertical burning tests showed excellent flame-retardancy of the CNF@HAP film. The insulation properties and combustion tests of the CNF@HAP film are presented in Figure 15a,b. The authors achieved an electrical output of 102 V in terms of open-circuit voltage, and a short-circuit current of 6.18 µA using the contactseparation mode. As the frequency increased from 0.5 to 3 Hz the output of the device also increased. As the ambient temperature increased from room temperature, the open-circuit voltage rose steadily up to 80 °C. However, beyond this temperature, the open-circuit voltage began to decline as the temperature continued to increase. Furthermore, CNF@HAP composite films demonstrated potential for use in high-temperature environments, retaining 90% of their triboelectric performance at 100 °C. The authors attached the TENG to the elbow of clothing as a self-powered sensor for fire rescue applications, as shown in Figure 15c. The radio signal of the self-powered sensor



ADVANCED MATERIALS

www.advmat.de

under varying temperatures, flame exposure, and water erosion is depicted in Figure 15d,e. The highly rough surface and unique microstructure significantly enhanced the triboelectric performance, while the densely packed cross-sectional structure created through this fabrication technique allowed air to fill it, providing heat insulation capabilities.

5.5. Carbon Materials

Numerous studies have highlighted the usage of carbon-based materials to enhance the efficacy of flame retardancy. Carbon black, carbon nanotubes (CNTs), and multi-wall graphene serve as flame retardants; however, their properties and types vary. CNTs remain among the most expensive carbon compounds due to the complexities of their production process. In contrast, graphite is a naturally occurring material that has been employed as a filler in the carbon layer structure of composite materials. Previous research has indicated that graphite nanoplatelets (GNP) or graphene can act as alternative fillers for CNTs in nanocomposites due to graphite's superior in-sheet properties. Seo et al. investigated various flame-retardant coating material composites using carbon materials such as xGnP, (natural graphite) NG, and expandable graphite (EG), which may be considered effective flame retardants for wood-based products.[121] Khose et al. devised a unique and simple approach for synthesizing graphene quantum dots (FR-GQD) using graphene oxide and phosphorus sources via hydrothermal synthesis. [122] This translucent FR-GQD solution-dipped cotton fabric maintained its original color.

Weldemhret et al. fabricated a fire-retardant TENG using PUF coated with phosphorus-doped mesoporous carbon (PMC).[123] A multilayer coating filled with PMC was deposited on PUF using the LBL method. To prepare the PMC, saccharose (SA) was employed as the carbon precursor, while phytic acid (PA) served as the precursor for phosphorus and carbon, and mesoporous silica (KIT-6) was used as a rigid template. Subsequently, a coating filled with negatively charged, alginate (AL)-stabilized PMC and positively charged chitosan (CH) was assembled onto the PUF cells via the LBL method. To assess the thermal properties of this TENG, cone calorimetry experiments were conducted on polyurethane foam (PUF), PUF coated with 3 BL (3 bilayers) of PMC, and PUF coated with 6 BL of PMC. The results indicated that as more layers were deposited, the concentration of CH and AL within the coating increased, leading to an increase in PHRR. Key fire resistance evaluation metrics, including HRR, rate of smoke release (RSR), total smoke release (TSR), peak CO₂ production rate, and peak CO production rate, were reduced by 56%, 48%, 29%, 35%, and 35%, respectively as shown in Figure 16a-h. This coating method enhances the flame retardancy of PUF while also improving the triboelectric effect. This method requires only a few layers and does not involve salt fortification, which is advantageous for scalability. The FRF-TENG generated respective open-circuit voltage and short-circuit current densities of 158 V and $2.26~\mu A~cm^{-2}$. This TENG was employed as a battery-free sensor for detecting various human motions.

Shie et al. fabricated hybridized nanogenerators based on a graphene-modified intumescent flame-retardant coating using the nanoimprinting method to design a self-powered thermal

sensor.[124] A hierarchical structure was formed by integrating a graphene-modified intumescent flame-retardant (GIFR) coating layer with a flexible and self-powered thermal sensor (FSTS). as shown in Figure 17a. The sensor combines PVDF-TrFE micro/nanofibers deposited by the NFES technique with an electrostatic friction layer made of PDMS. Figure 17b displays pure and oil-modified PVDF-TrFE nanofibers exhibiting porous morphology. Additionally, the GIFR coating was fully encapsulated in the sensor fabrication. Positive and negative charges arise from dipole moment balancing, with the application of external pressure leading to charge generation and, consequently, an electrical signal in the external circuit. Stability tests demonstrate the continuous power-generating performance of FSTS, which generates a power of 3160 nW for a load resistance of 13.3 M Ω . Based on these results, the FSTS can operate with high consistency. Unlike smoke and infrared flame detectors, the FSTS alert system is self-sufficient and utilizes graphene to enhance conductivity. This manufacturing approach offers a cost-effective solution for the mass production of nanostructures, as well as high output and scalable fabrication stability.

Recently, Chen et al. designed textiles-based TENG using flexible plasma-treated aramid nanofiber-based (p-ANFs) porous fibers (PFs). p-ANFs-based textile TENGs (t-TENGs) were constructed via wet-spinning, in-situ polymerization of polyaminopyrrole (H₂N-PPy)/(hydroxylated MWCNTs) HMWCNTs/p-ANFs fabrics, PTFE films, and copper films.[125] HMWCNTs/p-ANFs/DMSO solutions were injected into coagulation baths using a 23 G needle at a rate of 3 m min⁻¹. The hydrogel fibers were collected in stages using a CaCl₂ solution, an H2N-Py solution, and an acidic FeCl3 solution. The H₂N-PPy/HMWCNTs/p-ANFs PFs were then freeze-dried, as illustrated in Figure 17c. A hierarchical porous morphology was observed for the freeze-dried fibers. Optical images of p-ANFs and HMWCNTs/p-ANFs at various concentrations are presented in Figure 17d. The nanopores and micropores found in p-ANFs PFs captured a significant quantity of air, enhancing thermal insulation performance. The introduction of HMWCNTs and H₂N-PPy increases the energy required to break chemical bonds. The nitrogen atom produced by H₂N-PPy and the amide bond in p-ANFs acted as strong electron-donating groups, significantly enhancing the sensor's performance in harsh environments and its triboelectric output efficiency. p-ANFs-based textiles woven from p-ANFs-based PFs demonstrated good flexibility, breathability, flame retardancy, and heat insulation characteristics due to their stable hierarchical porous structure.

Among these, the TGA rate of the $\rm H_2N\text{-}PPy/HMWCNTs/p-ANFs$ PFs achieved 45% at 800 °C. The TENG generates 110 V, 15 µA, and 0.09 µC. Due to the abundance of amide bonds and thermal stability, the t-TENG demonstrated good output efficacy (80 V, 20 µA) and stability at high temperatures (120 °C), which was up to 40% higher than room temperature. Aromatic polyesters, such as aramid, are known to have poor UV resistance. However, studies have shown that p-ANFs PFs and HMWCNTs/p-ANFs PFs, even without a protective H2N-PPy layer, exhibited only slow degradation of benzene rings after 50 h of UV exposure. Furthermore, under extremely cold conditions, the t-TENGs demonstrated an ability to slow the drop in body temperature. Specifically, after 5 min at -40 °C, the t-TENG temperature increased from 19 to 22 °C. In addition, during the

15214095, 2025, 9, Downloaded from https://advanced.

onlinelibrary.wiley.com/doi/10.1002/adma.202415099 by Dægu Gyeongbuk Institute Of, Wiley Online Library on [20.03/2025]. See the Terms

onditions) on Wiley Online Library for rules of use; OA articles are governed by the applicable Creative Commons License

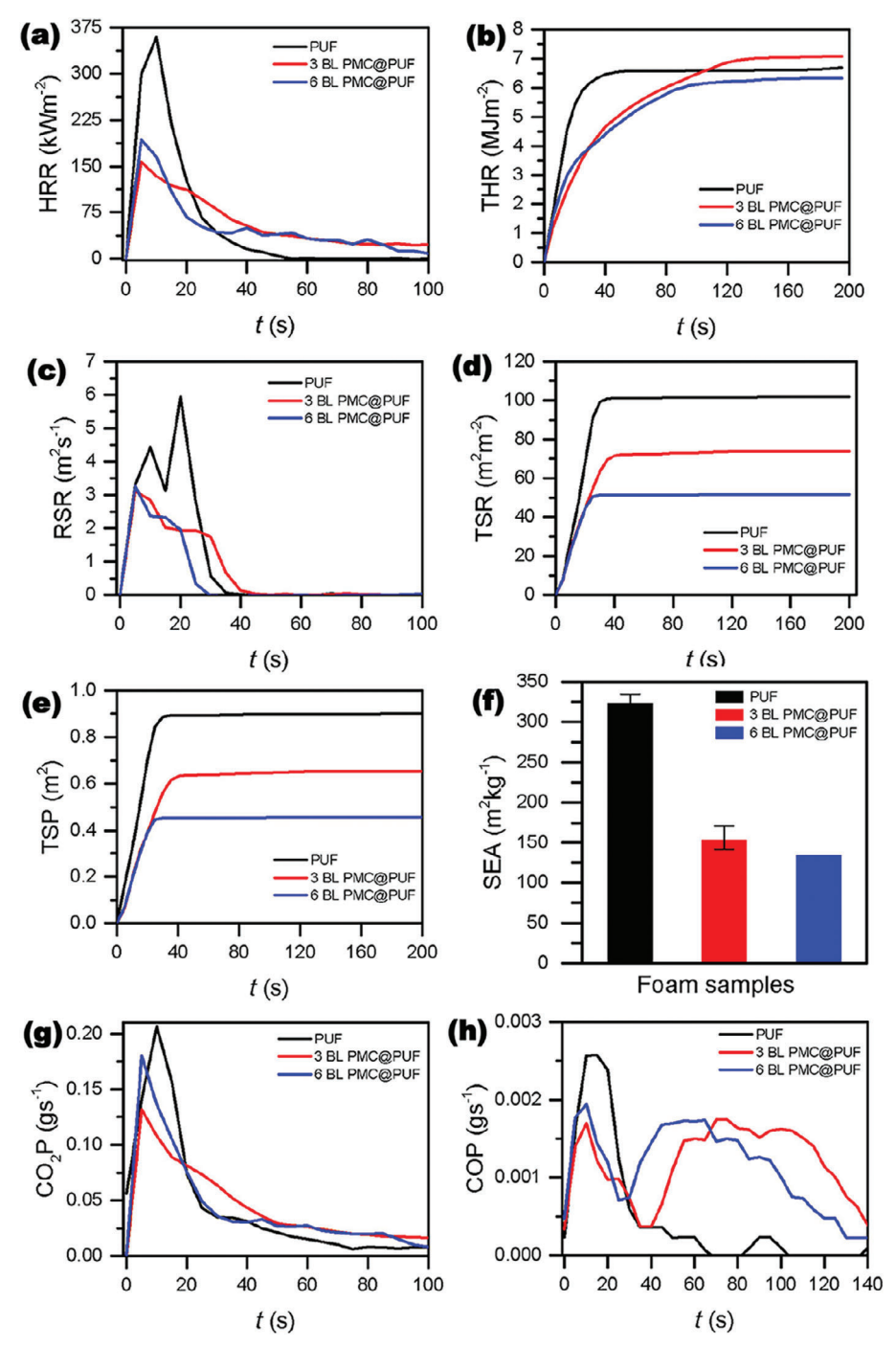


Figure 16. a) HRR, b) THR, c) RSR, d) TSR, e) TSP, f) SEA, g) CO₂P, and h) COP as a function of time for pristine (control) and coated PUFs. Reproduced with permission. [123] a—h) Copyright 2022, American Chemical Society.

jumping phase, the output signals of the t-TENGs remained more stable, although the frequency was lower. Walking led to a decline in output signals, which decreased as survivors became weaker, as seen in Figure 17e. An oscilloscope was utilized to continuously monitor the voltage at different contact periods to simulate long and short communications, such as Morse code. A message stating "CZC needs help" was generated using Morse code, as illustrated in Figure 17f.

6. Fabrication and Structural Integrity of Flame-Retardant Yarns

Ma et al. employed hollow spindle fancy twister technology to create 3D honeycomb-structured flame-retardant triboelectric fabric. [126] This technology is used in textile production to create specialized yarns with unique properties. In this process, a hollow spindle is utilized to twist and combine fibers continuously,

15214095, 2025, 9, Downloaded from https://advanced.onlinelibrary.wiley.com/doi/10.1002/adma.202415099 by Dægu Gyeongbuk Institute Of, Wiley Online Library on [20.03/2025]. See the Terms and Conditions (https://onlinelibrary.wiley.com/terms/

and-conditions) on Wiley Online Library for rules of use; OA articles are governed by the applicable Creative Commons License

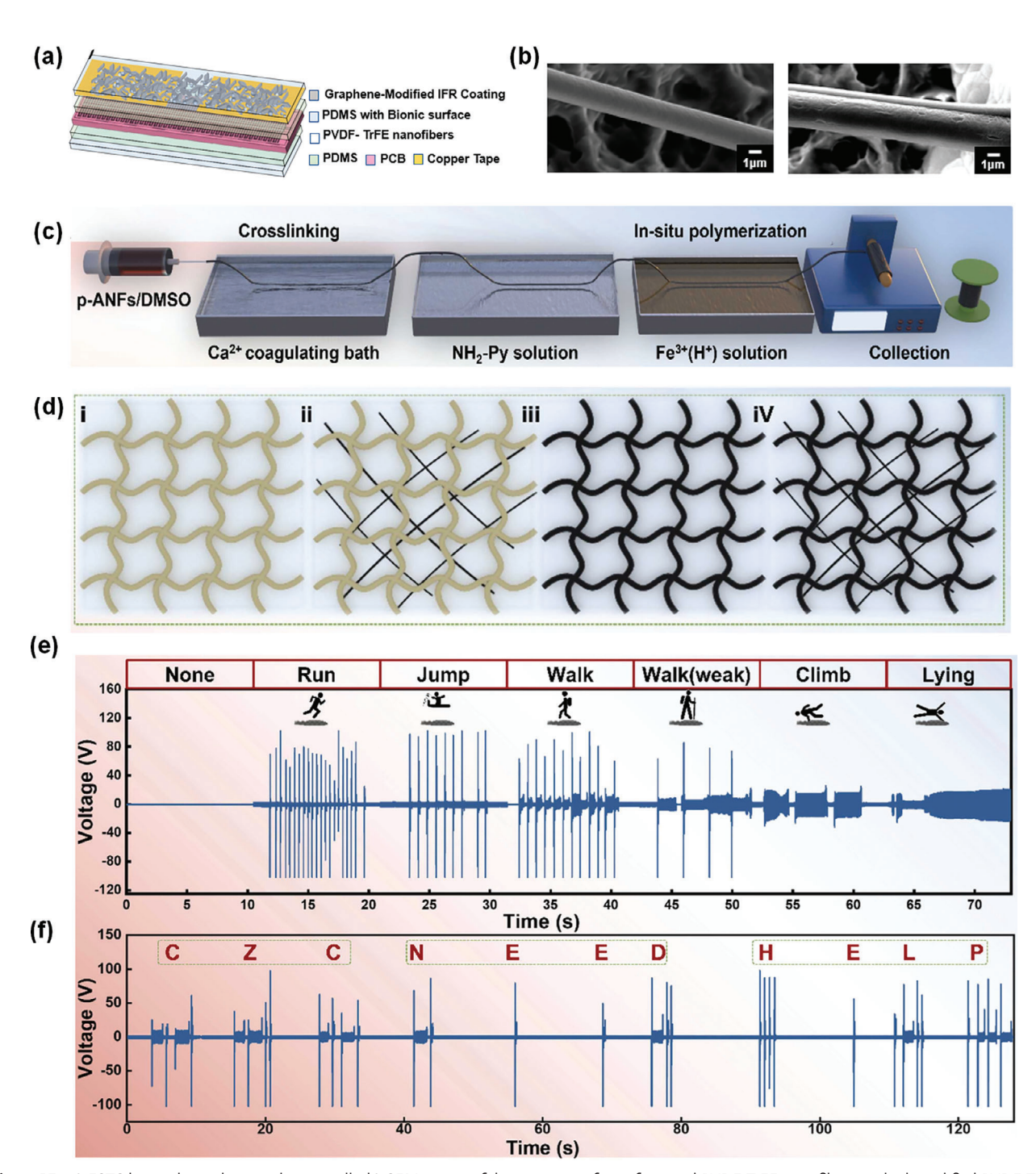


Figure 17. a) FSTS hierarchy is shown schematically. b) SEM image of the porous surface of original PVDF-TrFE nanofibers and oil-modified PVDF-TrFE nanofibers. a,b) Reproduced with permission. [124] Copyright 2023, American Chemical Society. c) Preparation process of H2N-PPy/HMWCNTs/p-ANFs PFs. d) Optical images of plasma-treated aramid nanofiber-based (p-ANFs) and HMWCNTs/p-ANFs at different concentrations. e) Output voltage of the survivors in different motion states. f) Morse code converted by t-TENGs friction power generation. c–f) Reproduced with permission. [125] Copyright 2024. Elsevier.

allowing for the production of yarns with specific characteristics such as fineness, strength, and texture, as shown in Figure 18a-f.

The F-TENG fabrics possess appropriate thickness and breathability, enhancing comfort for electronic textiles. The honeycomb structure is unique, comprising significant thickness and increased air permeability. The electrical output and performance varied among different fabric structures, with the twill weave structure exhibiting the highest output. Variations in electrical outputs were attributed to differences in fabric structure parameters, particularly the density of warp and weft yarns, which

15214095, 2025, 9, Downloaded from https

elibrary.wiley.com/doi/10.1002/adma.202415099 by Dægu Gyeongbuk Institute Of, Wiley Online Library on [20.03/2025]. See the Term

on Wiley Online Library for rules of use; OA articles are governed by the applicable Creative Commons

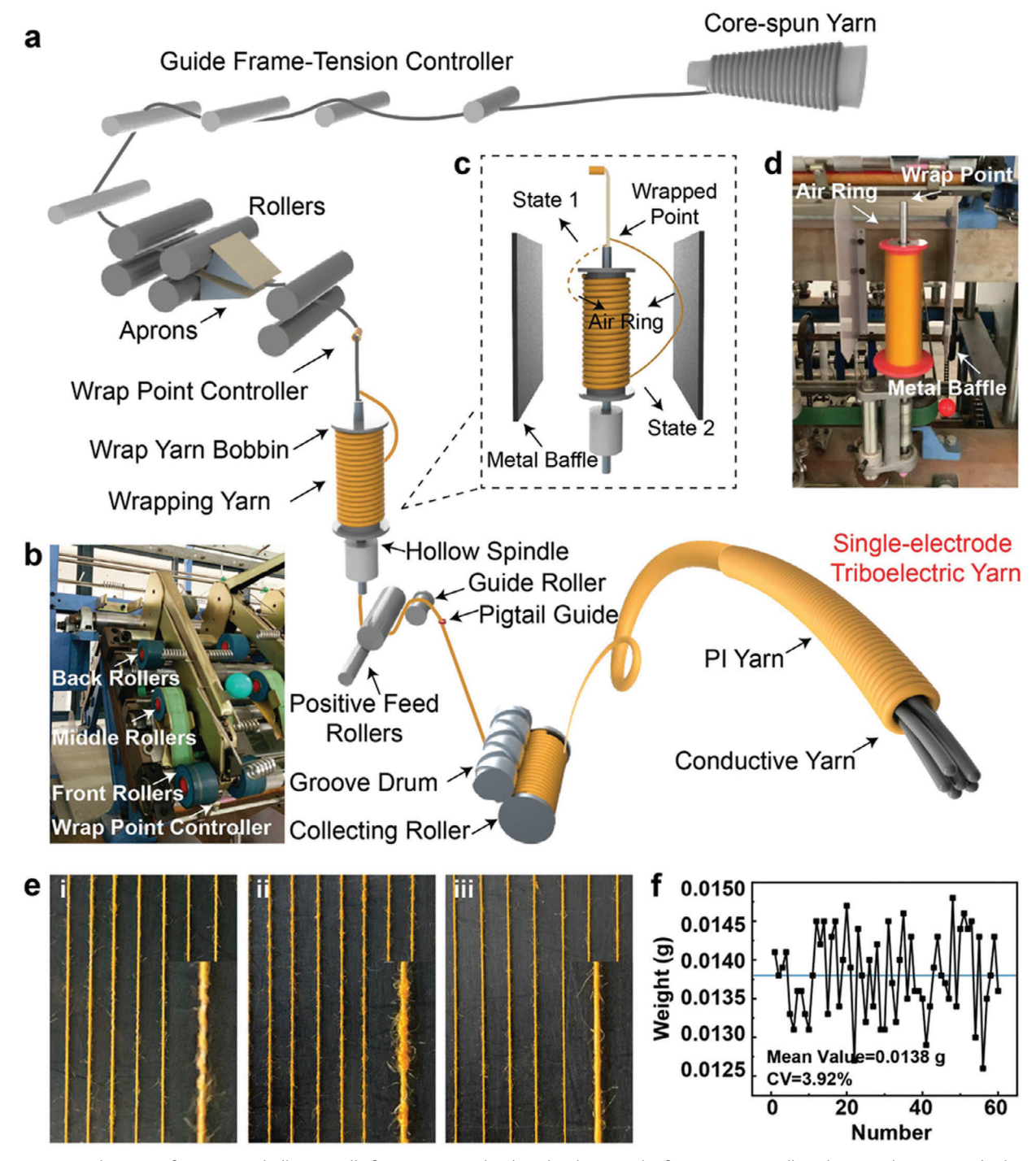


Figure 18. a) Schematic of continuous hollow spindle fancy twister technology. b) Photograph of core yarn controlling device. c,d) Device and schematic of the yarn wrapping area. e) Pictures of FRTYs by the blackboard method to characterize the yarn quality. f) Weight of the FRTYs by a quantitative test method to characterize yarn fineness and uniformity. a-f) Reproduced with permission. [126] Copyright 2020, Wiley.

can be controlled to manage charge output per unit area. The 3D F-TENG fabric, with its flame-retardant properties, noise reduction capabilities, and self-powered features, can be employed to create a safer indoor environment, aiding in firefighting and rescue operations, and providing real-time guidance for escape routes. This advanced manufacturing approach, which employs

hollow spindle fancy twister technology, is not only compatible with standard fabric processing techniques, but also efficient, scalable, and reproducible in the manufacture of complex 3D structures in textiles. This increases manufacturing efficiency and allows for the development of uniform, high-quality flameretardant materials tailored to individual fire escape and rescue



Table 2. Comparison table for various flame-retardant materials, fabrication methods, and electrical outputs.

Materials	Preparation method	TENG mode	Vol [V]	Cur [μA]	Power, power/current density	Refs.
PVDF and PVA/PPA-PEI	Solution-casting	Contact-separation	28.8	62.3	228.8 μW	[102]
PPMS-FEP	Polymerization and hot pressing	Contact-separation	230	_	182 mA m ⁻²	[103]
PTFE-coated fabric	LBL self-assembly	Contact separation	145	3.25	343.19 mW m^{-2}	[104]
SpinPTFE-coated fabric/ CS@MWCNT@PA	LBL self-assembly and soaking methods	Contact separation	85	-	141 mW m ⁻²	[105]
Urea-CNTs based shear stiffening elastomer (SSE).	Polymer blending and incorporation of additives	Contact separation	22.70	=	57.25 μW	[106]
Carbon fiber (CF)-reinforced liquid crystalline thermosetting (LCT)	One-pot multicomponent melt condensation procedure	Single-electrode mode	125.7	0.8	-	[107]
All-aromatic liquid crystalline poly (aryl ether ester) (LCP_{AEE})	One-pot melt polycondensation	Single-electrode mode	50	=	3.75 mA m ⁻²	[108]
Epoxy-based ion-gel films	Spin-coating	Contact separation	150	45	$300~\mu W~cm^2$	[110]
Ionic liquid-catalyzed high carbon-loaded polyurethane foam (PUF)	One-pot mixing and molding	Single-electrode mode	130.6	-	15.6 μA cm ⁻²	[112]
PAN nanofibers-graphene oxide nanosheets Carbon-aerogel nanocomposite	Sol-gel reaction, cross-linking polymerization	Single-electrode mode	80	-	25 μA m ⁻²	[114]
High-temperature silicon aerogel-BT-NF	Hydrolysis, gel-polymerization, solvent replacement, hydrophobic modification	Contact separation	135	-	31.9 mW m ⁻²	[115]
Black phosphorus (BP) and phytic acid (PA)- PVC	Vacuum filtration method	Contact separation	116	3.8	$3.02~{\rm mA~m^{-2}}$	[117]
PA/CS@A-MWCNTs nylon fabric	LBL self-assembly and soaking methods	Contact separation	≈200	-	173 mW m ⁻²	[118]
Polyurethane foam (PUF) coated with phosphorus-doped mesoporous carbon (PMC)	LBL deposition	Single electrode	158	-	2.26 μA cm ⁻²	[123]
Graphene-modified intumescent flame retardant (GIFR) flame-retardant coating-PVDF	Brush-painting and drying	Contact separation	11.8	1.11	3160 nW	[124]
Polyimide yarns	Modern spinning technology	Single electrode mode	6	_	$73.55 \; \mu W \; m^{-1}$	[126]
FR-PET filaments, pure PET filaments	High-speed machine braiding	Single electrode mode	12	0.36	3.0 Mw m ⁻²	[127]

needs. A comparison table of various flame-retardant materials, their preparation methods, TENG working modes, and their electrical outputs is shown in **Table 2**.

Cui et al. employed a high-speed machine braiding technique to create a flame-retardant Y-TENG (FRY-TENG), with FR-PET serving as the exterior friction layer and then wove the resulting yarns into an FRT-TENG. [127] The researchers used commercial silver-plated nylon yarn with low linear resistance (24 Ω cm $^{-1}$) and high ductility as core electrodes, braiding FR-PET yarn with permanent flame retardancy, and stable performance externally (Figure 19 a–d). They employed a single-electrode mode of TENG with an acrylic plate as the opposite triboelectric layer to obtain electrical output. At 2 Hz, the output current remains constant when the load resistance is less than 10 M Ω but decreases as it increases from 10 M Ω to 1 G Ω . The FRT-TENG remains unaffected after extinguishing a fire; 33.58% of the initial electrical output of the FRT-TENG remains constant at 200 °C, demonstrating the ef-

fectiveness of the TENG in operating across various temperature ranges, as shown in Figure 19e. Finally, in a home laundry scenario, the cleaning process was sustained for 20 min at 600 rpm, and after 20 washes, the energy harvesting capability of the TENG remained intact. This high-speed machine-braiding technology enhances flame-retardant triboelectric yarns and textiles by increasing structural strength, flexibility, flame resistance, and triboelectric performance, all while maintaining lightweight and comfort. These advantages make it a scalable, practical option for fire-resistant applications, particularly where safety, comfort, and stability are crucial.

7. Importance and Future Possible Applications

TENGs have emerged as promising energy harvesting devices, and incorporating flame-retardant materials into TENG designs opens a range of possible applications, offering both enhanced

15214095, 2025, 9, Downloaded from https:

library.wiley.com/doi/10.1002/adma.202415099 by Dægu Gyeongbuk Institute Of, Wiley Online Library on [20/03/2025]. See the Term

on Wiley Online Library for rules of use; OA articles are governed by the applicable Creative Commons License

(a) Winding roller FRY-TENG Conductive yarn Weaving FR-PET yarn FRT-TENG Machine bad (b) (d) (e) 30 24 $V_{oc}(V)$ **After Burning**

Figure 19. a) Schematic for fabrication strategy of FRY-TENG and FRT-TENG. b) Photograph of the FRY-TENG. c) Surface SEM image of the FRY-TENG. d) Cross-sectional SEM image of the FRY-TENG. e) The V_{OC} of the FRT-TRNG samples before and after burning (Inset are the images of the FRT-TENG samples before and after burning and their LED powering capability). a-e) Reproduced with permission. [127] Copyright 2023, Wiley.

safety and versatile functionality across various industries.[128] Here, we explore the significance and potential future applications of flame-retardant material-based TENGs.

Safety is paramount in numerous sectors, especially in environments prone to fire hazards, such as aerospace, automotive, and construction industries. Flame-retardant materials are engineered to inhibit or delay the spread of fire, thereby reducing the risk of ignition and flame propagation. [129,130] By integrating these materials into TENGs, researchers can develop self-powered sensors and devices that not only harvest energy but also possess inherent fire-resistant properties. This advancement ensures reliable operation even in high-risk settings, enhancing overall safety standards and minimizing the likelihood of catastrophic events.

In the aerospace industry, flame-retardant material-based TENGs hold significant promise for various applications. Aircraft components, including seats, panels, and insulation, can be equipped with self-powered sensors powered by TENGs. These sensors can monitor structural integrity, temperature, and environmental conditions, providing real-time data for improved maintenance and safety protocols. In addition, the energy harvested by TENGs can supplement power sources for onboard

Original

ADVANCED MATERIALS

systems, reducing reliance on traditional batteries and enhancing overall efficiency. $^{[131]}$

In the automotive sector, flame-retardant TENGs can revolutionize vehicle safety and performance. By integrating these devices into critical components such as seat cushions, airbags, and interior panels, manufacturers can create self-powered sensors capable of detecting impacts, changes in temperature, and air quality. In the event of a collision, TENG-powered sensors can trigger safety mechanisms and emergency response systems, enhancing overall occupant protection. Furthermore, the energy harvested by TENGs can contribute to the power supply for auxiliary systems, reducing fuel consumption and emissions.

In the construction industry, flame-retardant TENGs offer innovative solutions for building safety and sustainability. Smart building materials embedded with TENGs can detect structural stress, temperature fluctuations, and fire hazards in real-time, enabling proactive maintenance and risk mitigation strategies. [132] Moreover, the energy harvested by these devices can power wireless sensor networks for building automation and energy management, optimizing resource utilization, and reducing environmental impact. [133,134]

Beyond safety applications, flame-retardant material-based TENGs hold promise for environmental monitoring and wearable technology. By integrating these devices into clothing, footwear, and accessories, researchers can develop self-powered sensors for health monitoring, activity tracking, and environmental sensing.[135-137] For example, wearable TENGs could generate electricity from body movements, enabling continuous monitoring of vital signs and environmental pollutants without the need for external power sources.[138-140] Additionally, a fireretardant material is critical for wearable TENGs as they enhance user safety by reducing the risk of fire in close-contact devices that may encounter heat, electrical faults, or short circuits. It also ensures thermal stability, minimizing material degradation under changing temperatures and enabling a stable power supply, which is essential for wearable devices used in industrial or emergencies. [141,142] Fire-retardant TENGs also help meet safety regulations, strengthen consumer confidence, and increase the reliability of wearable devices. Importantly, selecting flame-retardant materials that maintain flexibility, biocompatibility, and triboelectric performance is crucial for comfortable and robust wearable devices.

Furthermore, flame-retardant TENGs can facilitate the development of self-powered electronic skins (e-skins) for robotics and prosthetics^[143–145] These flexible, fire-resistant sensors can provide tactile feedback, temperature sensing, and pressure detection capabilities, enhancing the functionality and safety of robotic systems and assistive devices.^[146,147] Additionally, the energy harvested by e-skins can power onboard electronics, reducing the need for bulky batteries and extending operational lifespan.

8. Recent Challenges and Future Improvements

Flame-retardant TENGs represent a promising fusion of renewable energy generation and fire safety. However, as with any emerging technology, they face a range of challenges ranging from efficiency limitations to scalability concerns. [148] Addressing these challenges and charting a course for future improvements is essential for unlocking the full potential of flame-retardant

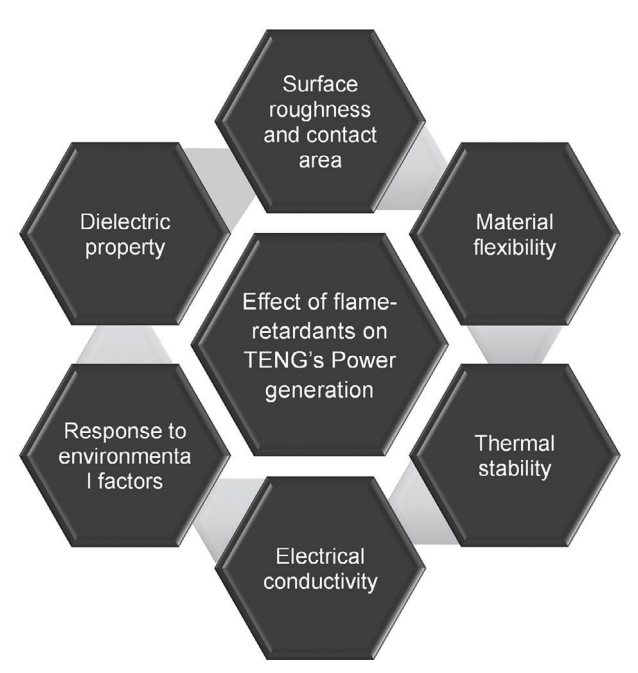


Figure 20. Factors affect the power generation of TENG by using flame-retardant materials.

TENGs. One of the primary challenges facing flame retardantbased TENGs is optimizing their efficiency without compromising fire safety. Traditional flame-retardant additives, while effective in enhancing fire resistance, can inadvertently hinder the triboelectric performance of TENG materials. For example, studies shed light on the addition of flame-retardant chemicals that can alter the material surface, leading to reduced triboelectric charge generation and transfer efficiency.^[149] To overcome this challenge, researchers are exploring innovative approaches to tailor flame-retardant formulations specifically for TENG applications. Recent advancements in nanomaterials have enabled the development of flame-retardant coatings with minimal impact on triboelectric performance. By leveraging nanotechnology, researchers can engineer flame-retardant materials at the molecular level, thereby fine-tuning their properties to meet the dual requirements of fire safety and high-performance energy generation.[150,151] Flame-retardant materials can also influence the power generation performance (Figure 20) of TENGs through the tailoring of several material properties, as described below:

8.1. Dielectric Properties

Flame retardants often modify the dielectric constant of TENG materials.^[152] Higher dielectric constants can enhance charge storage, potentially improving the TENG's power output. However, some flame-retardants may decrease the dielectric constant, leading to lower charge accumulation and reduced power generation.

8.2. Surface Roughness and Contact Area

Some flame-retardant materials or coatings alter the surface roughness, which is critical for TENG efficiency. A rougher



nunu advimat da

surface can increase the effective contact area and, therefore, the triboelectric charge density, boosting power generation. Conversely, smoother flame-retardant coatings could reduce friction and decrease power output.^[153]

8.3. Material Flexibility

The addition of flame-retardants may affect the flexibility of TENG materials. Reduced flexibility can hinder the contact-separation movement necessary for charge generation, especially in stretchable or wearable TENGs, potentially lowering power output. Flame-retardants that maintain or improve flexibility are preferable for high-performance applications.^[154]

8.4. Thermal Stability and Reliability

Flame-retardant materials enhance thermal stability, which can help TENGs maintain consistent performance at elevated temperatures. [155,156] This stability is essential for TENGs used in high-heat environments, although it may also introduce slight compromises in performance depending on the specific flame-retardant chemistry.

8.5. Electrical Conductivity

Some flame-retardant additives might exhibit slight conductivity, which can lead to charge dissipation if not carefully balanced, thereby reducing TENG efficiency. [157,158] Therefore, selecting non-conductive or insulating flame-retardants is critical to avoid power loss.

Another pressing challenge for flame-retardant TENGs is ensuring their scalability and cost-effectiveness for real-world applications. While laboratory-scale demonstrations have showcased the potential of TENG technology, transitioning from benchtop prototypes to commercially viable products requires overcoming numerous hurdles. These include optimizing manufacturing processes, sourcing cost-effective materials, ensuring long-term operations, and streamlining production workflows to meet market demands. To address these challenges, interdisciplinary collaboration between materials scientists, engineers, and industry is crucial.[159,160] By leveraging economies of scale and adopting innovative fabrication techniques such as electrospinning, coating, and additive manufacturing, researchers can significantly reduce the production costs of flame-retardant-based TENGs. Moreover, partnerships with manufacturers and regulatory bodies can help navigate compliance requirements and accelerate the commercialization of TENG-based fire safety solutions.[161]

Furthermore, ensuring the long-term durability and reliability of flame-retardant TENGs poses a significant challenge. Exposure to temperature fluctuations, moisture, and mechanical stress can degrade the performance of TENG devices over time, compromising their fire safety and energy generation capabilities. [162,163] Additionally, the integration of TENGs into real-world applications introduces additional complexities, such as compatibility with existing infrastructure and maintenance requirements. [164,165] To mitigate these challenges, researchers

are exploring novel materials and engineering approaches to enhance the durability of flame-retardant TENGs. For example, advancements in flexible and robust substrates, such as polymer composites and nanofiber matrices, can provide superior mechanical stability and environmental resilience. [166,167] Similarly, encapsulation techniques and protective coatings can help to maintain the fire-retardant properties of TENG devices, as illustrated in Figure 21.

In summary, the incorporation of flame-retardant fillers, hybrid composites, and surface treatments to improve fire resistance without compromising charge generation is necessary to balance the triboelectric and fire-retardant characteristics of materials. Both properties can be successfully maintained by combining triboelectric materials with flame-retardant polymers, adding nanoparticles, and optimizing the manufacturing process. By integrating triboelectrically active layers with flame-retardant outer layers, multilayer or gradient structures offer a calibrated method. Performance can be further enhanced by employing self-healing materials, flame-retardant cross-linking agents, and complex compounds that adapt to temperature fluctuations. Nanostructures such as graphene and complex thermoplastics like polyetheretherketone (PEEK) or polyimides are also key to increasing triboelectric efficiency and thermal stability.

Looking ahead, the future of flame-retardant TENGs holds immense promise, driven by ongoing research and technological innovation. Emerging trends such as the Internet of Things (IoT), smart cities, and wearable electronics present new opportunities for integrating TENG technology into diverse applications. [148,168,169] For instance, flame-retardant TENGs embedded in building materials could serve as self-powered sensors for fire detection and emergency response systems.[170,171] Moreover, advancements in materials science, energy harvesting techniques, and additive manufacturing are poised to revolutionize the design and performance of flame-retardant TENGs. By leveraging interdisciplinary expertise and embracing a holistic approach to innovation, researchers can overcome existing challenges and unlock new frontiers in sustainable energy generation and fire safety. By addressing efficiency limitations, scalability concerns, and durability issues through collaborative research and technological innovation, the future holds promise for flameretardant based TENGs. With continued progress, these innovative devices have the potential to pave the way toward safer, more sustainable, and resilient communities.

9. Conclusion

In conclusion, this review paper has illuminated the use of flame-retardant materials in TENGs, elucidating their properties, applications, challenges, and prospects. The integration of flame-retardant materials into TENG systems not only enhances their safety but also opens new avenues for energy harvesting in diverse environments. Through a systematic analysis of polymers, biomaterials, liquid polymers, aerogels, and carbon-based materials, this review underscores the versatility and potential of flame-retardant TENGs across various fields, from wearable electronics to environmental monitoring. Despite the promising advancements, several challenges, such as material compatibility, fabrication complexity, and environmental impact, remain to be addressed. However, with concerted research efforts and

15214095, 2025, 9, Downloaded

onlinelibrary.wiley.com/doi/10.1002/adma.202415099 by Dægu Gyeongbuk Institute Of, Wiley Online Library on [20/03/2025]. See the Terms

ons) on Wiley Online Library for rules of use; OA articles are governed by the applicable Creative Commons

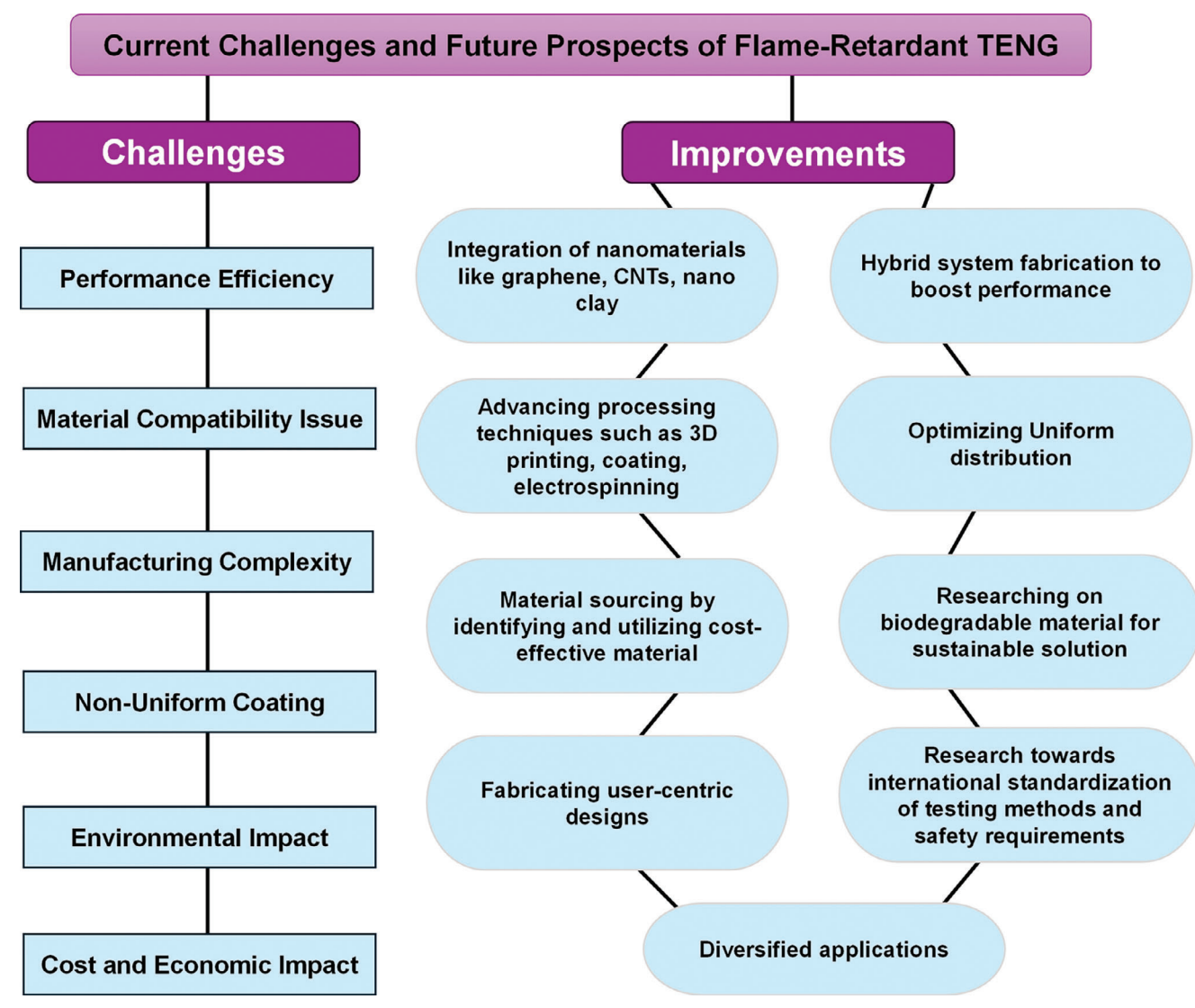


Figure 21. Current challenges and prospects of flame-retardant materials for diverse applications.

innovation, these obstacles can be overcome, leading to the development of highly efficient and environmentally friendly TENG devices. Overall, this review emphasizes the importance of flame retardancy in TENG technology and sets the stage for future advancements in this rapidly evolving field.

Acknowledgements

This work was supported by the National Research Foundation of Korea (RS-2024-00346135 and RS-2024-00431411). V.V. thanks the Department of Science and Technology, India for the financial support through the PURSE program (SR/PURSE/2023/196). K.M. thanks the Silesian University of Technology (Gliwice, Poland) for the financial support through the pro-quality Rector's grant No. 14/010/RGJ25/0018 and statutory research grant No. BK-208/RIF1/2025.

Conflict of Interest

The authors declare no conflict of interest.

Keywords

carbon-based materials, flame-retardant materials, safety devices, triboelectric nanogenerator

> Received: October 4, 2024 Revised: December 30, 2024 Published online: January 21, 2025

^[1] J. Zhu, M. Zhu, Q. Shi, F. Wen, L. Liu, B. Dong, A. Haroun, Y. Yang, P. Vachon, X. Guo, EcoMat 2020, 2, e12058.

^[2] Z. L. Wang, Adv. Energy Mater. 2020, 10, 2000137.

^[3] Z. L. Wang, Rep. Prog. Phys. 2021, 84, 096502.

^[4] S. Niu, Z. L. Wang, Nano Energy 2015, 14, 161.

^[5] Y. Zi, J. Wang, S. Wang, S. Li, Z. Wen, H. Guo, Z. L. Wang, Nat. Commun. 2016, 7, 10987.

^[6] T. Cheng, Q. Gao, Z. L. Wang, Adv. Mater. Technol. 2019, 4, 1800588.



www.advmat.de

- [7] J. Luo, W. Gao, Z. L. Wang, Adv. Mater. 2021, 33, 2004178.
- [8] S. Hajra, S. Panda, H. Khanberh, V. Vivekananthan, E. Chamanehpour, Y. K. Mishra, H. J. Kim, Nano Energy 2023, 115, 108729.
- [9] S. Panda, S. Hajra, Y. Oh, W. Oh, J. Lee, H. Shin, V. Vivekananthan, Y. Yang, Y. K. Mishra, H. J. Kim, Small 2023, 19, 2300847.
- [10] S. Panda, S. Hajra, H. G. Kim, H. Jeong, P. Achary, S. Hong, B. Dudem, S. R. P. Silva, V. Vivekananthan, H. J. Kim, J. Mater. Chem. B 2023, 11, 10147.
- [11] J. Zhao, Y. Shi, Adv. Funct. Mater. 2023, 33, 2213407.
- [12] J. Wen, B. Chen, W. Tang, T. Jiang, L. Zhu, L. Xu, J. Chen, J. Shao, K. Han, W. Ma, Adv. Energy Mater. 2018, 8, 1801898.
- [13] W. Xu, M.-C. Wong, J. Hao, Nano Energy 2019, 55, 203.
- [14] J. Chu, W. Wu, Y. Wei, Z. L. Wang, X. Chen, L. Zhang, Adv. Funct. Mater. 2024, 34, 2402520.
- [15] L. Feng, S. Xu, T. Sun, C. Zhang, J. Feng, L. Yao, J. Ge, Adv. Fiber Mater. 2023, 5, 1478.
- [16] X. Zhong, P. Sun, R. Wei, H. Dong, S. Jiang, J. Mater. Chem. A 2022, 10. 15080.
- [17] Y. Pang, S. Chen, J. An, K. Wang, Y. Deng, A. Benard, N. Lajnef, C. Cao, Adv. Funct. Mater. 2020, 30, 2003598.
- [18] H. Song, S. Panda, S. Hajra, S. Hwang, J. Jo, N. Kim, B. K. Panigrahi, J. Yu, S. M. Jeong, H. J. Kim, Energy Technol. 2024, 12, 2400424.
- [19] S. Das, A. Chowdhury, S. W. Ali, ACS Appl. Electron. Mater. 2024, 6, 2093.
- [20] X. Zhang, J. Hu, Q. Yang, H. Yang, H. Yang, Q. Li, X. Li, C. Hu, Y. Xi, Z. L. Wang, Adv. Funct. Mater. 2021, 31, 2106527.
- [21] J. Lai, Y. Ke, Z. Cao, W. Xu, J. Pan, Y. Dong, Q. Zhou, G. Meng, C. Pan, F. Xia, Nano Today 2022, 43, 101437.
- [22] S. Panda, H. Jeong, S. Hajra, P. M. Rajaitha, S. Hong, H. J. Kim, Sens. Actuators, B 2023, 394, 134384.
- [23] A. Babu, K. Ruthvik, P. Supraja, M. Navaneeth, K. U. Kumar, R. R. Kumar, K. Prakash, N. Raju, J. Mater. Sci.: Mater. Electron. 2023, 34, 2195
- [24] A. Chen, C. Zhang, G. Zhu, Z. L. Wang, Adv. Sci. 2020, 7, 2000186.
- [25] X. Tao, X. Chen, Z. L. Wang, Energy Environ. Sci. 2023, 16, 3654.
- [26] S. Roy, S. Maiti, J. Appl. Polym. Sci. 2001, 81, 785.
- [27] C. E. Hobbs, Polymers 2019, 11, 224.
- [28] Y. F. Lv, W. Thomas, R. Chalk, S. Singamneni, *Mater. Today: Proc.* 2020, 33, 5720.
- [29] J. Davis, M. Huggard, J. Vinyl Addit. Technol. 1996, 2, 69.
- [30] S. Fu, C. Hu, Adv. Funct. Mater. 2024, 34, 2308138.
- [31] D. A. Villamil Watson, D. A. Schiraldi, *Polymers* **2020**, *12*, 849.
- [32] W. Zhan, L. Li, L. Chen, Q. Kong, M. Chen, C. Chen, Q. Zhang, J. Jiang, Prog. Org. Coat. 2024, 192, 108483.
- [33] F. Wang, N. Wu, M. Wang, S. Deng, H. Jia, Polym. Degrad. Stab. 2024, 227, 110843.
- [34] Y. Liu, J. Zhang, Y. Ren, G. Zhang, X. Liu, H. Qu, Prog. Org. Coat. 2022, 163, 106599.
- [35] A. Beaugendre, S. Degoutin, S. Bellayer, C. Pierlot, S. Duquesne, M. Casetta, M. Jimenez, Coatings 2018, 8, 448.
- [36] J. Xiang, Y. Zhang, B. Zhang, L. Yuan, X. Liu, Z. Cheng, Y. Yang, X. Zhang, Z. Li, Y. Shen, Energy Environ. Sci. 2021, 14, 3510.
- [37] L. Wang, M. Sánchez-Soto, J. Fan, Z. P. Xia, Y. Liu, Polym. Adv. Technol. 2019, 30, 1807.
- [38] M. Farooq, M. H. Sipponen, A. Seppälä, M. Österberg, ACS Appl. Mater. Interfaces 2018, 10, 27407.
- [39] L. Zuo, W. Fan, Y. Zhang, L. Zhang, W. Gao, Y. Huang, T. Liu, Compos. Sci. Technol. 2017, 139, 57.
- [40] C. Cao, B. Yuan, Polym. Adv. Technol. 2021, 32, 2159.
- [41] S. Araby, B. Philips, Q. Meng, J. Ma, T. Laoui, C. H. Wang, Compos. B 2021, 212, 108675.
- [42] X. Wang, E. N. Kalali, J.-T. Wan, D.-Y. Wang, Prog. Polym. Sci. 2017, 69, 22.

- [43] D. P. Durkin, M. J. Gallagher, B. P. Frank, E. D. Knowlton, P. C. Trulove, D. H. Fairbrother, D. M. Fox, J. Therm. Anal. Calorim. 2017, 130, 735.
- [44] W. Lin, Y. Yuan, L. Xu, W. Wang, Molecules 2024, 29, 1858.
- [45] J. Luo, Z. L. Wang, EcoMat 2020, 2, e12059.
- [46] Y. Song, N. Wang, Y. Wang, R. Zhang, H. Olin, Y. Yang, Adv. Energy Mater. 2020, 10, 2002756.
- [47] S. Hajra, S. Panda, S. Song, B. K. Panigrahi, P. Pakawanit, S. M. Jeong, H. J. Kim, *Nano Energy* 2023, 114, 108668.
- [48] J. Jo, S. Panda, N. Kim, S. Hajra, S. Hwang, H. Song, J. Shukla, B. K. Panigrahi, V. Vivekananthan, J. Kim, J. Sci. Adv. Mater. Devices 2024, 9. 100693.
- [49] K. Ruthvik, A. Babu, P. Supraja, M. Navaneeth, V. Mahesh, K. U. Kumar, R. R. Kumar, B. M. Rao, D. Haranath, K. Prakash, *Mater. Lett.* 2023, 350, 134947.
- [50] M. Rakshita, N. Madathil, A. A. Sharma, P. P. Pradhan, D. P. Kasireddi AK, U. K. Khanapuram, R. K. Rajaboina, H. Divi, ACS Appl. Electron. Mater. 2024, 6, 1821.
- [51] W.-G. Kim, D.-W. Kim, I.-W. Tcho, J.-K. Kim, M.-S. Kim, Y.-K. Choi, ACS Nano 2021, 15, 258.
- [52] R. Dharmasena, K. Jayawardena, C. Mills, R. Dorey, S. Silva, *Nano Energy* 2018, 48, 391.
- [53] C. Wu, A. C. Wang, W. Ding, H. Guo, Z. L. Wang, Adv. Energy Mater. 2019, 9, 1802906.
- [54] S. Panda, S. Hajra, H.-G. Kim, P. G. R. Achary, P. Pakawanit, Y. Yang, Y. K. Mishra, H. J. Kim, ACS Appl. Mater. Interfaces 2023, 15, 36096.
- [55] R. T. Leon, P. C. Sherrell, J. I. Michel, J. Bullock, J. D. Berry, A. V. Ellis, ChemSusChem 2024, 17, 202400366.
- [56] Y. Bai, H. Feng, Z. Li, Cell Rep. Phys. Sci. 2022, 3, 101108.
- [57] Z. L. Wang, L. Lin, J. Chen, S. Niu, Y. Zi, Triboelectric Nanogenerators. Green Energy and Technology, Springer, Cham, Switzerland 2016, pp. 23-47.
- [58] X. Yin, D. Liu, L. Zhou, X. Li, C. Zhang, P. Cheng, H. Guo, W. Song, J. Wang, Z. L. Wang, ACS Nano 2018, 13, 698.
- [59] H. Zhang, L. Quan, J. Chen, C. Xu, C. Zhang, S. Dong, C. Lü, J. Luo, Nano Energy 2019, 56, 700.
- [60] A. Babu, L. Bochu, S. Potu, R. Kaja, N. Madathil, M. Velpula, A. Kulandaivel, U. K. Khanapuram, R. K. Rajaboina, H. Divi, ACS Sustain. Chem. Eng. 2023, 11, 16806.
- [61] Q.-Z. Guo, C.-P. Liu, Nano Energy 2020, 76, 104969.
- [62] R. Kumar, A. K. Goyal, Y. Massoud, Results Eng. 2024, 22, 102108.
- [63] Z. L. Wang, L. Lin, J. Chen, S. Niu, Y. Zi, Triboelectric Nanogenerators. Green Energy and Technology, Springer, Cham, Switzerland 2016, pp. 91–107.
- [64] S. Niu, Y. Liu, S. Wang, L. Lin, Y. S. Zhou, Y. Hu, Z. L. Wang, Adv. Funct. Mater. 2014, 24, 3332.
- [65] S. Niu, Y. Liu, S. Wang, L. Lin, Y. S. Zhou, Y. Hu, Z. L. Wang, Adv. Mater. 2013, 25, 6184.
- [66] Z. L. Wang, L. Lin, J. Chen, S. Niu, Y. Zi, Triboelectric Nanogenerators. Green Energy and Technology, Springer, Cham, Switzerland 2016, pp. 49–90.
- [67] W. He, W. Liu, J. Chen, Z. Wang, Y. Liu, X. Pu, H. Yang, Q. Tang, H. Yang, H. Guo, Nat. Commun. 2020, 11, 4277.
- [68] G. Li, J. Wang, Y. He, S. Xu, S. Fu, C. Shan, H. Wu, S. An, K. Li, W. Li, Energy Environ. Sci. 2024, 17, 2651.
- [69] Y. Yu, H. Li, X. Zhang, Q. Gao, B. Yang, Z. L. Wang, T. Cheng, Joule 2024, 8, 1855.
- [70] S. Wang, L. Lin, Y. Xie, Q. Jing, S. Niu, Z. L. Wang, Nano Lett. 2013, 13, 2226.
- [71] W. Yang, J. Wang, X. Wang, P. Chen, Friction 2024, 12, 1828.
- [72] S. Badatya, M. K. Patel, M. K. Gupta, Nanoscale 2024, 16, 4176.
- [73] T. Jiang, X. Chen, C. B. Han, W. Tang, Z. L. Wang, Adv. Funct. Mater. 2015, 25, 2928.

www.advmat.de

- [74] H. Wang, Y. Kurokawa, J. Wang, W. Cai, J. H. Zhang, S. Kato, N. Usami, Small 2024, 20, 2308531.
- [75] S. Niu, Y. Liu, X. Chen, S. Wang, Y. S. Zhou, L. Lin, Y. Xie, Z. L. Wang, Nano Energy 2015, 12, 760.
- [76] S. Wang, Y. Xie, S. Niu, L. Lin, Z. L. Wang, Adv. Mater. 2014, 26, 2818.
- [77] Y. Hu, X. Li, Y. Gao, Z. Zhao, X. Liu, L. He, B. Zhang, L. Zhou, Z. L. Wang, J. Wang, Adv. Energy Mater. 2024, 14, 2400672.
- [78] J.-w. Gu, G.-c. Zhang, S.-l. Dong, Q.-y. Zhang, J. Kong, Surf. Coat. Technol. 2007, 201, 7835.
- [79] X.-H. Shi, X.-L. Li, Y.-M. Li, Z. Li, D.-Y. Wang, Composites, Part B 2022, 233, 109663
- [80] Y. Ding, K. Kwon, S. I. Stoliarov, R. H. Kraemer, Proc. Combust. Inst. 2019, 37, 4247.
- [81] M. M. S. Mohd Sabee, Z. Itam, S. Beddu, N. M. Zahari, N. L. Mohd Kamal, D. Mohamad, N. A. Zulkepli, M. D. Shafiq, Z. A. Abdul Hamid, *Polymers* 2022, 14, 2911.
- [82] X. Qiu, Z. Li, X. Li, Z. Zhang, Chem. Eng. J. 2018, 334, 108.
- [83] J. W. Gilman, Flame Retardant Polymer Nanocomposite (Eds: A. B. Morgan, C. A. Wilkie), Wiley, Hoboken, NJ, USA 2007, pp. 67-87.
- [84] M. Zhi, X. Yang, R. Fan, S. Yue, L. Zheng, Q. Liu, Y. He, Polym. Degrad. Stab. 2022, 201, 109976.
- [85] B. W. Liu, H. B. Zhao, Y. Z. Wang, Adv. Mater. 2022, 34, 2107905.
- [86] T. Sai, S. Ran, Z. Guo, P. Song, Z. Fang, SusMat 2022, 2, 411.
- [87] H. Xie, X. Lai, H. Li, X. Zeng, Polym. Degrad. Stab. 2016, 130, 68.
- [88] Y. Pan, Z. Guo, S. Ran, Z. Fang, J. Appl. Polym. Sci. 2020, 137, 47538.
- [89] Y.-M. Li, S.-L. Hu, D.-Y. Wang, Compos. Commun. 2020, 21, 100405.
- [90] L. Chen, Y. Dong, Y.-Q. Tong, M.-J. Liu, G.-J. Yang, Corros. Commun.
- 2023, 12, 19.[91] A. Dasari, Z.-Z. Yu, G.-P. Cai, Y.-W. Mai, Prog. Polym. Sci. 2013, 38,
- [91] A. Dasari, Z.-Z. Yu, G.-P. Cai, Y.-w. Mai, *Prog. Polym. Sci.* **2013**, *38*, 1357.
- [92] B. Xu, X. Wu, W. Ma, L. Qian, F. Xin, Y. Qiu, J. Anal. Appl. Pyrolysis 2018, 134, 231.
- [93] F. Laoutid, L. Bonnaud, M. Alexandre, J.-M. Lopez-Cuesta, P. Dubois, Mater. Sci. Eng. R: Rep. 2009, 63, 100.
- [94] B. Schartel, K. Kebelmann, Flame Retardant Polymeric Materials: A Handbook, 1st ed., (Eds: Y. Hu, X. Wang), Taylor & Francis CRC Press, Boca Raton, FL, USA 2019, pp. 35–55.
- [95] L. Chen, Z. Xu, F. Wang, G. Duan, W. Xu, G. Zhang, H. Yang, J. Liu, S. Jiang, Compos. Commun. 2020, 20, 100355.
- [96] M. Sabet, Polym.-Plast. Technol. Mater. 2024, 63, 1794.
- [97] J. R. Xavier, S. Vinodhini, B. Ramesh, Polym. Degrad. Stab. 2024, 227, 110847.
- [98] H. A. Alhazmi, M. Albratty, Pharmaceuticals 2023, 16, 291.
- [99] M. Bar, R. Alagirusamy, A. Das, Fibers Polym. 2015, 16, 705.
- [100] L.-Y. Lv, C.-F. Cao, Y.-X. Qu, G.-D. Zhang, L. Zhao, K. Cao, P. Song, L.-C. Tang, Mater. Sci. Eng. R: Rep. 2022, 150, 100690.
- [101] S. S. Ray, L. T. Temane, J. T. Orasugh, Graphene-Bearing Polymer Composites: Applications to Electromagnetic Interference Shielding and Flame-Retardant Materials, Springer Nature, Cham, Switzerland 2024, pp. 43–118.
- [102] X. Chen, A. Yusuf, J. S. del Rio, D.-Y. Wang, Nano Energy 2021, 81, 105656.
- [103] W. Ma, T. Long, H. Wu, J.-H. Zhang, Y. Lyu, M. Zhao, J. Li, Q. Zhang, C. Zhou, C. Zhang, Chem. Eng. J. 2024, 480, 148198.
- [104] R. Cheng, K. Dong, L. Liu, C. Ning, P. Chen, X. Peng, D. Liu, Z. L. Wang, ACS Nano 2020, 14, 15853.
- [105] G. Zhang, C. Liu, L. Yang, Y. Kong, X. Fan, J. Zhang, X. Liu, B. Yuan, J. Colloid Interface Sci. 2024, 658, 219.
- [106] H. Chen, J. Zhou, S. Liu, S. Wang, X. Gong, Nano Energy 2022, 102, 107634.
- [107] M. Qadeer, Q. Guan, Q. Guo, A. Rahman, M. Z. Nawaz, J. Zhou, S. Zhu, Adv. Mater. Technol. 2022, 7, 2200002.
- [108] Q. Guan, X. Lu, Y. Chen, H. Zhang, Y. Zheng, R. E. Neisiany, Z. You, Adv. Mater. 2022, 34, 2204543.

- [109] X. Qi, Y. Liu, L. Yu, Z. Yu, L. Chen, X. Li, Y. Xia, Adv. Sci. 2023, 10, 2303406.
- [110] Y. Kim, D. Lee, J. Seong, B. Bak, U. H. Choi, J. Kim, Nano Energy 2021, 84, 105925.
- [111] Z. Zhou, Q. Guan, S. Zhong, Q. Wang, Y. Xu, Z. Cao, H. Xu, ACS Appl. Polym. Mater 2022, 4, 5813.
- [112] T. G. Weldemhret, D.-W. Lee, Y. T. Park, J. I. Song, Chem. Eng. J. 2022, 450. 137982.
- [113] Z. Qian, R. Li, J. Guo, Z. Wang, X. Li, C. Li, N. Zhao, J. Xu, Nano Energy 2019, 64, 103900.
- [114] A. Ahmed, M. F. El-Kady, I. Hassan, A. Negm, A. M. Pourrahimi, M. Muni, P. R. Selvaganapathy, R. B. Kaner, Nano Energy 2019, 59, 336.
- [115] J. Hu, Y. Qian, F. Wei, J. Dai, D. Li, G. Zhang, H. Wang, W. Zhang, Nano Energy 2024, 121, 109229.
- [116] J. Luo, X. Shi, P. Chen, K. Han, X. Li, X. Cao, Z. L. Wang, *Mater. Today Phys.* 2022, 27, 100798.
- [117] R. Wang, J. Ma, S. Ma, Q. Zhang, N. Li, M. Ji, T. Jiao, X. Cao, Chem. Eng. J. 2022, 450, 137985.
- [118] G. Zhang, Y. Kong, L. Wang, S. Nie, X. Liu, B. Yuan, Compos. Commun. 2024, 46, 101854.
- [119] B. Tang, Z.-P. Deng, J.-M. Wu, Y.-Y. Zhao, Q.-W. Tan, F. Song, X.-L. Wang, Y.-Z. Wang, J. Mater. Chem. A 2023, 11, 26716.
- [120] Q. Duan, Z. Zhang, J. Zhao, J. He, W. Peng, Y. Zhang, T. Liu, S. Wang, S. Nie, Nano Energy 2023, 117, 108851.
- [121] H. J. Seo, S. Kim, W. Huh, K.-W. Park, D. R. Lee, D. W. Son, Y.-S. Kim, J. Therm. Anal. Calorim. 2016, 123, 1935.
- [122] R. V. Khose, D. A. Pethsangave, P. H. Wadekar, A. K. Ray, S. Some, Carbon 2018, 139, 205.
- [123] T. G. Weldemhret, D.-W. Lee, M. Prabhakar, Y. T. Park, J. I. Song, ACS Appl. Nano Mater. 2022, 5, 12464.
- [124] C. Y. Shie, C.-C. Chen, H. F. Chen, Y. H. Lin, C. H. Liu, Y.-K. Fuh, T. Li, ACS Appl. Nano Mater. 2023, 6, 2429.
- [125] Z. Chen, C. Zhou, W. Xia, X. Yin, Z. Wang, X. Fu, D. Liu, J. Lv, R. Liu, Z. Peng, Nano Energy 2024, 123, 109359.
- [126] L. Ma, R. Wu, S. Liu, A. Patil, H. Gong, J. Yi, F. Sheng, Y. Zhang, J. Wang, J. Wang, Adv. Mater. **2020**, *32*, 2003897.
- [127] X. Cui, A. Li, Z. Zheng, H. Wu, R. Wang, Adv. Mater. Technol. 2023, 8, 2202116.
- [128] S. Divya, S. Hajra, S. Panda, V. Vivekananthan, K. Mistewicz, H. J. Kim, T. H. Oh, Chem. Phys. Lett. 2023, 826, 140648.
- [129] F. Uddin, J. Ind. Text. 2016, 45, 1128.
- [130] E. W. Madyaratri, M. R. Ridho, M. A. Aristri, M. A. R. Lubis, A. H. Iswanto, D. S. Nawawi, P. Antov, L. Kristak, A. Majlingová, W. Fatriasari, *Polymers* 2022, 14, 362.
- [131] T. Bhatta, O. Faruk, M. R. Islam, H. S. Kim, S. S. Rana, G. B. Pradhan, A. Deo, D.-S. Kwon, I. Yoo, J. Y. Park, *Nano Energy* **2024**, *127*, 109793.
- [132] Y. Pang, T. He, S. Liu, X. Zhu, C. Lee, Adv. Sci. **2024**, 11, 2306574.
- [133] Y. K. Tan, S. K. Panda, Sustain. Wirel. Sens. Networks 2010, 2010, 15.
- [134] D. K. Sah, T. Amgoth, Inf. Fusion 2020, 63, 223.
- [135] Z. Li, Q. Zheng, Z. L. Wang, Z. Li, Research 2020, 2020, 8710686.
- [136] M. Zhu, Q. Shi, T. He, Z. Yi, Y. Ma, B. Yang, T. Chen, C. Lee, ACS Nano 2019, 13, 1940.
- [137] M. Zhu, Z. Yi, B. Yang, C. Lee, Nano Today 2021, 36, 101016.
- [138] A. A. Mathew, A. Chandrasekhar, S. Vivekanandan, *Nano Energy* 2021, 80, 105566.
- [139] Y. Su, G. Chen, C. Chen, Q. Gong, G. Xie, M. Yao, H. Tai, Y. Jiang, J. Chen, Adv. Mater. 2021, 33, 2101262.
- [140] Y. Yang, X. Guo, M. Zhu, Z. Sun, Z. Zhang, T. He, C. Lee, Adv. Energy Mater. 2023, 13, 2203040.
- [141] A. Yusuf, Z. Li, X. Yuan, D. Y. Wang, Small Methods 2022, 6, 2101428.
- [142] E. E. Mbamalu, U. E. Chioma, A. Epere, Proc. Indian Natl. Sci. Acad. 2024, 1.
- [143] Y.-C. Lai, R. Liu, M. Xu, C. Zhao, Handbook of Triboelectric Nanogenerators, Springer, Cham, Switzerland 2023, pp. 1–52.

of use; OA articles are governed by the applicable Creative Commons

www.advancedsciencenews.com



www.advmat.de

- [144] B. Zhang, Y. Jiang, B. Chen, H. Li, Y. Mao, *Nano Energy Adv.* **2024**, *4*, 45.
- [145] L. Liu, M. Wu, W. Zhao, J. Tao, X. Zhou, J. Xiong, Adv. Funct. Mater. **2024**, *34*, 2308353.
- [146] Q. Zhang, C. Xin, F. Shen, Y. Gong, Y. Zi, H. Guo, Z. Li, Y. Peng, Q. Zhang, Z. L. Wang, Energy Environ. Sci. 2022, 15, 3688.
- [147] S. K. Karan, S. Maiti, J. H. Lee, Y. K. Mishra, B. B. Khatua, J. K. Kim, Adv. Funct. Mater. 2020, 30, 2004446.
- [148] Y. Tang, H. Fu, B. Xu, Adv. Compos. Hybrid Mater. 2024, 7, 102.
- [149] Y. Mi, Z. Zhao, H. Wu, Y. Lu, N. Wang, Polymers 2023, 15, 4383.
- [150] C. Zhi, S. Shi, H. Wu, Y. Si, S. Zhang, L. Lei, J. Hu, Adv. Mater. 2024, 36, 2401264.
- [151] R. Chen, X. Jia, H. Zhou, S. Ren, D. Han, S. Li, Z. Gao, Mater. Today 2024, 75, 359.
- [152] R. Wang, D. Zhuo, Z. Weng, L. Wu, X. Cheng, Y. Zhou, J. Wang, B. Xuan, J. Mater. Chem. A 2015, 3, 9826.
- [153] M. Yu, T. Zhang, J. Li, J. Tan, X. Zhu, Mater. Des. 2023, 225, 111529.
- [154] C. Shen, R. Shao, W. Wang, X. Wu, B. Zhou, L. Zhao, A. Siddique, Z. Xu, Eur. Polym. J. 2024, 220, 113478.
- [155] L. Sun, H. Wang, W. Li, J. Zhang, Z. Zhang, Z. Lu, P. Zhu, C. Dong, Cellulose 2021, 28, 3789.
- [156] P. Wang, L. Xia, R. Jian, Y. Ai, X. Zheng, G. Chen, J. Wang, *Polym. Degrad. Stab.* 2018, 149, 69.
- [157] Y.-T. Li, W.-J. Liu, F.-X. Shen, G.-D. Zhang, L.-X. Gong, L. Zhao, P. Song, J.-F. Gao, L.-C. Tang, Compos. B 2022, 238, 109907.

- [158] N. F. Attia, A. A. El Ebissy, M. A. Hassan, Polym. Adv. Technol. 2015, 26, 1551.
- [159] J. Li, J. Cai, J. Yu, Z. Li, B. Ding, Adv. Funct. Mater. 2023, 33, 2303249.
- [160] J. E. Regis, A. Renteria, S. E. Hall, M. S. Hassan, C. Marquez, Y. Lin, *Materials* 2021, 14, 4521.
- [161] B. Shao, Z. Chen, H. Su, S. Peng, M. Song, Int. J. Mol. Sci. 2024, 25, 6152
- [162] R. Cao, Y. Liu, H. Li, Z. Shen, F. Li, X. Jia, C. Chen, R. Liu, C. Luo, W. Yang, SusMat 2024, 4, e196.
- [163] S. Zhu, Y. Liu, G. Du, Y. Shao, Z. Wei, J. Wang, B. Luo, C. Cai, X. Meng, S. Zhang, *Nano Energy* **2024**, *124*, 109449.
- [164] A. Babu, D. Mandal, ACS Appl. Energy Mater. 2024, 7, 822.
- [165] L. Jiang, X. Liu, J. Lv, G. Li, P. Yang, Y. Ma, H. Zou, Z. L. Wang, Energy Environ. Sci. 2024, 17, 3700.
- [166] X. Hou, J. Chen, Z. Chen, D. Yu, S. Zhu, T. Liu, L. Chen, ACS Nano 2024, 18, 11525.
- [167] , M. Haque, S. M. Islam, K. R. U. Labib, Heliyon 2024, 10, e24692.
- [168] A. Haque, K. Bharath, M. Amir, Z. Khan, Smart Cities: Power Electronics, Renewable Energy, and Internet of Things, CRC Press, Boca Raton, FL, USA 2024, pp. 66–95.
- [169] M. P. Nguyen, N. D. Huynh, T. T. Luu, D. Choi, J. Phys.: Energy 2024, 6, 022001.
- [170] R. Wang, M. Ji, X. Jin, Q. Zhang, T. Jiao, Nano Futures 2022, 6, 022003.
- [171] Z. Zhao, Y. Lu, Y. Mi, J. Meng, X. Cao, N. Wang, Micromachines 2022, 13, 1586.



Swati Panda is currently a doctoral student at Daegu Gyeongbuk Institute of Science and Technology (DGIST), South Korea. She received her Bachelor's degree from Utkal University, Odisha, India in 2018. She pursued her Master's degree from Siksha O Anusandhan University, India with a specialization in Biotechnology in 2020. Her research interests focus on developing self-powered biosensors and biodegradable/biocompatible materials-based piezoelectric/triboelectric energy harvesters.



Sugato Hajra is currently a postdoctoral researcher at Daegu Gyeongbuk Institute of Science and Technology (DGIST) South Korea. He received a Bachelor in Technology degree from Siksha O Anusandhan University, India, in 2017. He pursued his M. Tech. degree with a specialization in VLSI and Embedded Systems at Siksha O Anusandhan University, and also served as a joint researcher at the Advanced Multifunctional and Materials Laboratory in the Institute of Technical Education and Research, Bhubaneswar, India in 2019. He received the Ph.D. degree in the Department of Robotics and Mecharonics Engineering in 2024 from DGIST, South Korea. His research interests mainly include lead-free piezoelectric/ multiferroics materials, metal—organic frameworks, solid-state electronic devices, and hybrid energy harvesters.



Hoe Joon Kim is currently an Associate Professor in Robotics Engineering with the Daegu Gyeongbuk Institute of Science and Technology (DGIST), Daegu, South Korea, and also holds a courtesy appointment in the Information and Communication Engineering Department at DGIST. He received the B.S. degree from Johns Hopkins University, Baltimore, MD, USA, in 2009, and the M.S. and Ph.D. degrees from the University of Illinois at Urbana—Champaign, Urbana, IL, USA, in 2011 and 2015, respectively, all in mechanical engineering. His research interests focus on piezoelectric MEMS resonators for RF wireless communication, nanogenerators, chemical/physical sensing, environmental monitoring, and emerging nanomaterials.